NTNU – Trondheim
Norwegian University of
Science and Technology

Greenland ice mass balance using GRACE gravity data

Vegar Schwartz

NORGES TEKNISK-
NATURVITENSKAPELIGE UNIVERSITET
INSTITUTT FOR BYGG, ANLEGG OG TRANSPORT

Oppgavens tittel:	Dato: 24.01.2014		
Greenland mass balance using GRACE gravity data	Antall sider (inkl. bilag): 67		
	Masteroppgave	x	Prosjektoppgave	

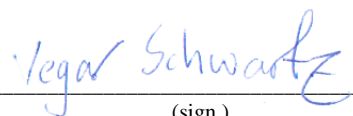| Navn: |
|---|
| Vegar Schwartz |
| Faglærer/veileder: |
| Hossein Nahavandchi |
| Eventuelle eksterne faglige kontakter/veiledere: |
| |

Ekstrakt:

Grønlands massebalanse er studert med data fra satellittparet «Gravity Recovery and Climate Experiment» (GRACE). Månedlige data fra januar 2003 til desember 2012 er benyttet fra de tre leverandørene av Nivå-2-data. Disse er «Jet Propulsion Laboratory» (JPL), «GeoForschungsZentrum» (GFZ) og «Center for Space Research» (CSR). Den lineære trenden i denne studien tyder på en massebalanse på -181±11, -172±10 og -183±11 gigatonn per år for de tre forskningssentrene. Viktige korreksjonsfaktorer som er blitt anvendt er gravitasjonslekkasjeeffekten, justering for landheving fra forrige istid og ikke-isotropisk utglatting.

Denne tesen gir også et innblikk i noe av den matematiske bakgrunnen for fysikalsk geodesi, samt hvordan dette kan brukes til å spore variasjoner i gravitasjonsfeltet. Metoden for denne anvendelsen er beskrevet, og naturlige antakelser underveis er forklart. Resultater for korreksjoner, viktige langtidstrender og plott gjennom ulike tidsspenn fra de tre dataleverandørene er angitt. I tillegg vises det til resultater fra andre viktige studier, og disse blir sammenlignet med denne studiens funn. Avslutningsvis nevnes noen styrker og svakheter ved studien. Etter forfatterens kunnskap er dette den første studien som estimerer massebalansen, eller issmeltingen på Grønland ved å benytte GRACE Nivå-2-data som er dekorrelert med ikke-isotropisk filtrering.

Stikkord:

1. GRACE
2. Greenland
3. Mass Balance
4. Ice loss

_____
(sign.)

Title

Greenland mass balance using GRACE gravity data

Type of project

Master thesis

Project description

The Gravity Recovery and Climate Experiment (GRACE) satellite gravity mission has been providing valuable information regarding Earths gravity field. GRACE not only maps the Earths static gravity field but it also measures temporal variation in the Earths gravity field to a scale of several hundred kilometers and with a period of around one month. In recent years, several research groups have used GRACE data to estimate the rate of ice mass change over Greenland. The purpose of this thesis is to demonstrate the extent and magnitude of Greenland ice sheet surface melting between 2003 and 2012 . The thesis should contain a description of the theory, GRACE gravity data used in the computations, and an explanation of the estimates for ice mass variability over Greenland. Following subjects should be studied:

Different releases and levels of monthly GRACE gravity data

Filtering (smoothing) effect for the GRACE data

Correction terms

Ice mass loss/gain estimates

Comparison of the estimated values with available results

Comment on the results

Supervisors

Main supervisor: Hossein Nahavandchi
Assisting supervisor: Gholamreza Joodaki

Abstract

The mass balance of Greenland has been assessed with data from the Gravity Recovery and Climate Experiment (GRACE) satellite mission. Monthly data has been used through the time span of the study; January 2003 – December 2012. Level 2 data from three providers has been used. These are the Jet Propulsion Laboratory (JPL), GeoForschungsZentrum (GFZ) and the Center for Space Research (CSR). The linear trend in this study points to -181±11 $^{\text{Gt}}/_{\text{yr}}$, -172±10 $^{\text{Gt}}/_{\text{yr}}$ and -183±11 $^{\text{Gt}}/_{\text{yr}}$ for the three data providers respectively. Notable corrections applied to improve the accuracy of this study are gravity leakage correction, adjustment for post-glacial rebound and non-isotropic smoothing filtering.

This master thesis also gives an insight into some of the mathematical background of physical geodesy and how this can be applied to use GRACE data to track changes in the gravity field. The methodology of applying this theory is explained in-depth with explanations of some natural assumptions along the way. Results are presented from correction calculations, important secular trend graphs and different time series plots of data from the three data providers. These results are compared to the works of other mentionable authors in the field of polar mass redistribution. Lastly, the thesis enlists some noteworthy strengths and weaknesses of the conducted study. To the author's knowledge, this is the first ice mass loss estimation of Greenland using GRACE level 2 Release 05 data decorrelated by non-isotropic filtering.

Preface

The subject of this thesis was chosen collaboratively between the candidate and the supervisor. The candidate has used GRACE data earlier, in assessments of different geoid models for Norway, and he has programmed tasks similar to those needed in this thesis in previous projects. The topic of Greenland ice mass balance was chosen as this has a profound purpose to our world, and even if a lot of studies have been published earlier, more are still needed to increase the certainty with which we can estimate the mass balance as more and better data becomes available.

As the project progressed, it became clear that the results of this thesis would be good material for one, maybe two scientific articles. This, of course, contributed to inspiring and motivating the candidate into checking and double-checking every result, and to put some extra effort into the presentation of the results, as the same figures will be used in scientific publications.

Acknowledgements

I would like to express my sincere gratitude to those who provided me with the possibility and ability to do this project. I would like to thank my main supervisor Hossein Nahavandchi for inspiring me to pursue physical geodesy and for his contributions to the field I have been exploring during the course of this project. The learning curve through this process has been very steep, thanks to my supervisor's enthusiastic lecturing – both on the core material and everything else I could ask about.

I would also like to acknowledge with great appreciation the help and expertise always available from Gholamreza Joodaki. Without his generous software contributions and his patient sharing of own experiences through his PhD process, this project would by no means have been possible for me to complete on time.

Contents

List of Figures

List of Tables

Glossary

Term	Explanation
A_{lm}, B_{lm}	Coefficients describing gravitational potential
C_{20}	The term describing the Earth's oblateness
CSR	Center for Space Research
CPU	Central Processing Unit
DDK	Decorrelation Filter by Jürgen Kusche
DLR	Deutche Forschungsanstalt für Luft und Raumfahrt
EGM	Earth Gravitational Model. Most recent version is 2008
GFZ	GeoForschungsZentrum. Located at Potsdam
GGM	GRACE Gravity Models. Used to compute the geoid
GGM(s)	Geoid model using only satellite data
GIA	Glacial Isostatic Adjustment. See PGR
GMT	Generic Mapping Tools. Scientific plotting
GRACE	Gravity Recovery and Climate Experiment
Gton	10^9 ton
ICE-5G	Model of post-glacial rebound
IPCC	Intergovernmental Panel on Climate Change
JPL	Jet Propulsion Laboratory. Institute at NASA
K-band	Distance measurement tools aboard GRACE
LaTeX	Typesetting software
Level 2	GRACE raw data processed by either JPL, GFZ or CSR
Mass balance	The fluctuation of matter in or out of an area
Matlab	Programming language
NMA2012v30	Norwegian Geoid model by Statens Kartverk
PGR	Post-glacial rebound, Land rise from after the last ice age
RL04, RL05	The two latest release iteration of Level 2 GRACE data
SLR	Satellite Laser Ranging
TikZ	Graphing toolbox for LaTeX
Truncation	Omitting of high frequencies due to noise
UTCSR	University of Texas, Center for Space Research
σ	Surface density ($\rho \times$ Area)
ϕ, λ	Latitude and longitude

x

Chapter 1

Introduction

Over the course of the last decade, scientists from a wide variety of fields have displayed a concern for the state of the climate of the Earth. According to the Intergovernmental Panel on Climate Change (IPCC) there is no longer any reasonable doubt to the human contributions to the climate change [27]. Determining these changes is; however, painstakingly difficult and involves complex and advanced observations. One such contribution comes from the monitoring of the constantly changing mass distribution of the Earth. These variations happens; of course, naturally with seasons, storms, earthquakes et cetera [32]. On the other hand, a warmer climate might also lead to a mass redistribution of the vast landlocked ice caps in the polar regions [3, 7, 17, 28, 34, 35, 33, 40]. If floating icebergs melt, this will not directly influence the global sea level, but if landlocked ice melts, it will inevitably cause the water level to rise [12]. It is therefore of great interest to observe mass redistribution over the great ice continents, such as Greenland and Antarctica.

Figure 1.1 shows the great extent of the Greenland island. Almost 80 percent of its two million km^2 surface is covered with ice, some places over three kilometers thick. The total amount of ice on Greenland has been estimated to 2.85 million km^3. Rapid changes in the ice mass would result in a global water rise, which in turn would cause immeasurable problems for

Figure 1.1: Greenland and the northern cap. Image courtesy of NASA

cities close to the sea [10]. Some populated islands could vanish completely if the water should rise a few meters. Monitoring the mass change has traditionally been very difficult because of the size of the areas and the accuracy of available measurement accuracy. With satellite gravimetry, this has become increasingly feasible. After just over a decade in flight, the Gravity Recovery and Climate Experiment (GRACE) has provided global mass change information with a high resolution. Moreover, new methods are constantly being developed to increase the accuracy and reduce the errors of these measurements [16]. New studies on the polar mass changes are published with every new data set and every iteration of improved methodology. In the last few years, some scientists have also suggested that the ice cap decline is accelerating by studying the GRACE data [17, 35]. Hopefully, studies like this can contribute to a greater understanding of the complex climate on the planet we all share.

GRACE data is now currently in its fifth release [9], and all previous raw data has been brought back from the archives and recomputed using the latest correction techniques. The data is published as global monthly harmonic coefficients that can be used to study any great mass change on the planet. The GRACE satellite pair celebrated their 10th anniversary in 2012 [25], and have now had their lifespan extended until the GRACE Follow-On

(FO) mission will be launched in 2017 to provide even more accurate data [2]. The GRACE and GRACE-FO missions are joint partnerships between NASA, the Deutche Forschungsanstalt für Luft und Raumfahrt (DLR) and the University of Texas Center for Space Research (UTCSR) [16]. The providers of processed Level 2 data are the Jet Propulsion Laboratory (JPL), GeoForschungsZentrum (GFZ) and the University of Texas (CSR). Data from all these three providers are available at the homepages of GFZ, http://icgem.gfz-potsdam.de/ICGEM/.

Several authors have previously published estimations of the mass balance in the polar regions. Some noteworthy findings from other authors are included in this thesis. These have not only provided interesting results, but also paved the way for better estimation techniques. In the process of writing this thesis, a numerous different techniques for computing the mass balance from different authors have been considered.

This project aims to reveal the trends in the mass balance on Greenland using the latest data and the latest methods of correction. This would not have been possible, had it not been for the incredible amount of work done by other scientists. Following this introduction, Chapter 2 gives an overview of the fundamentals of physical geodesy, the principles of using GRACE data for the computations necessary to this thesis and the theories of corrections. Chapter 3 provides insight into how the computations were performed and how some assumptions and choices were made. In Chapter 4, the results are presented and discussed. The findings are also compared to work by other authors that have been studied through the course of this project. Lastly, Chapter 5 summarized the thesis and adds some final thoughts.

Chapter 2

Theory

In this chapter, an introduction to some necessary theory will be given. The main goal is to show that Newton's general law of gravitation can be transformed in such a way that it is possible to measure the gravitational field of the Earth from satellite data. Furthermore, some information will be given on the satellites that are used for these measurements. We will also look into some correction that are needed to accurately determine the mass balance. These corrections are mainly the gravity leakage effects and the post-glacial rebound. In addition, we also study the improvements in the latest iteration of GRACE data (RL05) and look into the theory of replacing coefficient C_{20}; the Earth's dynamic oblateness. Finally, a short description of the two main filtering techniques is given.

2.1   Mathematical foundation

This section will give a brief overview of how one can develop mathematical methods for describing some aspects of the physical world. We begin by expanding Newton's law of gravitation with the goal of developing differential equations that can be solved by separation of variables. We then describe a model field on which we can study the measurable disturbing potential

before finally deriving Bruun's formual and the fundamental differentiation equation of geodesy. These can be applied to the task sought to be solved in this thesis. This chapter does not involve relativistic considerations, even though this has to be taken into account when studying the precise GPS receivers and oscillators aboard the GRACE satellites [19]. Along the way, we will also have a quick peek at the definition of geoid height – a very useful property that can be computed from GRACE data.

2.1.1   Newton's law of gravitation

Newton's general law of gravitation

$$F = G\frac{Mm}{r^2} \tag{2.1}$$

describes the general behavior of the attractions of bodies, where G is the universal gravitational constant, a general property of any mass with a value of approximately $6.674{\times}10^{-11}\,\mathrm{m^3kg^{-1}s^{-2}}$ shown through experiments [15]. One can expand, or rewrite this formula into a triple integral with respect to the local density variations in the bigger mass M as following:

$$\vec{F}_{\beta \to A} = \vec{F}(\vec{r}_A) = Gm \iiint_\beta \frac{\rho(\vec{r})}{|\vec{r} - \vec{r}_A|^3}(\vec{r} - \vec{r}_A)d\beta \tag{2.2}$$

Here, the mass M has been substituted by a vector field of an infinite number of vectors $\vec{r}$ pointing from the mass points inside the Earth. This formula; however, requires a knowledge of the the density $\rho(\vec{r})$ of all the points inside the Earth's body, β. This is a very difficult – if not impossible task to solve, so instead we work towards finding a way of expressing the gravity potential in another, easier solvable way. It can be shown that the Earth is irrotational (meaning that the work needed to overcome gravity is independent of path), and the result of this is that one can consider the vector field in eq. 2.2 as a scalar field, thus simplifying the computations to come.

2.1.2   Poisson and Laplace

Poisson's equation, also called *the fundamental, partial differential equation of second order for gravity potential,*

$$\nabla^2 W(\vec{r}_A) = -4\pi G \rho(\vec{r}_A) + 2\omega^2 \tag{2.3}$$

describes gravity and the centrifugal force as vectors, i.e. acceleration due to the forces. The ∇^2 denotes the divergence of this vector field and ω is the angular spin velocity of the Earth. This spin is zero at the poles and has its maximum along the equator. In empty space outside the body we want to measure, we get

$$\nabla^2 W(\vec{r}_A) = 2\omega^2 \tag{2.4}$$

as the density ρ in empty space is 0. If we for now omit the centrifugal force, and only study the gravitational component of eq. 2.4, we get the Laplace equation

$$\nabla^2 W_g = \Delta W_g = 0 \tag{2.5}$$

whose solutions are called harmonic functions. The gravitational potential then, is such a function and we are going to seek a solution to this using separation of variables, also called the Fourier technique, in a spherical coordinate system of (r, ϕ, λ). The Laplace equation can be described in such a coordinate system by a partial differential equation as

$$\nabla^2 W_g(\vec{r}_A) = \frac{2}{r_A} \frac{\partial W_g}{\partial r_A} + \frac{\partial^2 W_g}{\partial r_A^2} + \frac{\cot \phi}{r_A^2} \frac{\partial W_g}{\partial \phi} + \frac{1}{r_A^2} \frac{\partial^2 W_g}{\partial \phi^2} + \frac{1}{r_A^2 \sin^2 \phi} \frac{\partial^2 W_g}{\partial \lambda^2} = 0. \tag{2.6}$$

2.1.3 Fourier's separation of variables

For the time being, we can simplify eq. 2.6 by writing it as a product of some functions R, T and L, or simply R and J

$$W_g(r, \phi, \lambda) = R(r) \cdot T(\phi) \cdot L(\lambda) = R(r) \cdot J(\phi, \lambda) \qquad (2.7)$$

In eq. 2.7, R describes W_g approximately normal to the Earth's surface and J depicts variations in the potential of the surface. Through solving the differential equations one can derive from eq. 2.6, the following results can be shown to hold true for the functions J and R

$$J(\phi, \lambda) = \sum_{l=0}^{\infty} \sum_{m=0}^{l} (\bar{A}_{lm} \cos m\lambda + \bar{B}_{lm} \sin m\lambda) \bar{P}_{nm}(\cos \phi) \qquad (2.8)$$

$$R_2 = r^{-(l+1)} \Rightarrow r \to \frac{r}{a} \Rightarrow R_2 = \left(\frac{r}{a}\right)^{-(l+1)} = \left(\frac{a}{r}\right)^{l+1} \qquad (2.9)$$

where $\bar{P}_{nm}$ denotes the normalized Legendre polynomials described in section 2.1.7. The subtext of R_2 in eq. 2.9 indicates that there are in fact two solutions to the differential equation for R, but only the second solution is useful to this purpose. The semi major axis of the reference ellipsoid is denoted by a. The final equation for the external gravitational potential we are now arriving at is identical to eq. 2.2, but we have substituted the more or less immeasurable density ρ with two new sets of unknown coefficients $\bar{A}_{lm}$ and $\bar{B}_{lm}$:

$$W_g^e(r, \phi, \lambda) = \sum_{l=0}^{\infty} \sum_{m=0}^{l} \left(\frac{a}{r}\right)^{l+1} \left[\bar{A}_{lm} \cos m\lambda + \bar{B}_{lm} \sin m\lambda\right] \bar{P}_{lm}(\cos \phi)$$

$$(2.10)$$

The last thing to consider in this section is how one can solve the coefficients $\bar{A}_{lm}$ and $\bar{B}_{lm}$. To do this, we need two more equations. We can define a boundary sphere $s(R = a)$ where the gravitational potential is known and write

$$\nu(\phi, \lambda) = W_g(a, \phi, \lambda) \tag{2.11}$$

where $\bar{A}_{lm}$ and $\bar{B}_{lm}$ can be computed by developing ν into spherical harmonics over a model sphere s using the following two formulas

$$\bar{A}_{jk} = \oiint_s \nu(\theta, \lambda)\bar{Y}_{jk}^C(\phi, \lambda)ds \tag{2.12}$$

and

$$\bar{B}_{jk} = \oiint_s \nu(\theta, \lambda)\bar{Y}_{jk}^S(\phi, \lambda)ds \tag{2.13}$$

where the new coefficients $\bar{Y}_{jk}^C$ and $\bar{Y}_{jk}^S$ will be possible to measure.

2.1.4 Model gravity field

Instead of measuring the values of the coefficients $\bar{A}_{lm}$ and $\bar{B}_{lm}$ directly, we now describe a mathematical approximation model of the Earth, so that we can instead measure the differences between the model and the physical world. This procedure has two significant advantages: (1) Measurements on differences has a much smaller sensitivity to errors than measurements of the full physical values, and (2) we don't have any equipment to measure the values directly anyway. We introduce the disturbing potential T instead of W and define

$$T(\vec{r}_a) = W(\vec{r}_a) - U(\vec{r}_a) \tag{2.14}$$

where U is a mathematical model. This model has to meet certain criteria not covered here. Analog to the model potential U, we define a model gravity on the geocentric ellipsoid γ_0 such that

$$\Delta g = g_0 - \gamma_0 \tag{2.15}$$

where Δg is the difference between the normal physical gravity g_0 and the normal model gravity γ_0. Bruun's formula gives us another important

9

relationship between the physical world and the mathematical world. If N is the geoid height, Bruun showed that

$$N = \frac{T}{\gamma_0} \tag{2.16}$$

which in turn, by defining H as local height, can be extended into *the fundamental differentiation equation of geodesy*

$$g_0 - \gamma_0 = \Delta g = -\frac{\partial T}{\partial H} + \frac{1}{\gamma_0}\frac{\partial \gamma}{\partial H}T \tag{2.17}$$

2.1.5 Dirichlet's principle

The reason why we took the time to develop this equation, is that is solves one of Dirichlet's boundary value problems. Dirichlet's principle says that if a harmonic function f is unknown outside a boundary but known on the boundary, there exists a unique and derivable solution outside the boundary as well. Eq. 2.17 is an example of a mixed-type boundary value problem where we have a combination of values for f and its normal derivative df. In our case, the general function f is the disturbing potential T, and this is solvable according to Dirichlet's principle.

2.1.6 Geoid height

We now have the knowledge to combine Bruun's formula (eq. 2.16) with the equation of external gravitational potential (eq. 2.10) to express the geoid height N as

$$N(r, \phi, \lambda) = \frac{GM}{R\gamma} \sum_{l=0}^{\infty} \left(\frac{a}{r}\right)^l \sum_{m=0}^{l} \left(\bar{A}_{lm} \cos m\lambda + \bar{B}_{lm} \sin m\lambda\right) \bar{P}_{lm}(\sin \phi) \tag{2.18}$$

where $\gamma = 9.81\,\mathrm{m/s^2}$. If N is computed globally, it describes the shape of the geoid. The global geoid heights allows us to assess the differences in the gravity potential of the world, which is close to the goal of this thesis. A good model of the geoid has a wide array of applications itself, but for this project, we need to continue a bit further. What we want is after all a method of computing varying density from GRACE data.

Figure 2.1 is highly exaggerated and shows anomalies in the geoid. In reality the variations due to the geoid anomalies are in the area of [-100,80]m with respect to the mean Earth radius. The accuracy of an Earth model can be thought of as iterative: The first step ($n = 1$) will describe a sphere with a given radius. The second step ($n = 2$) describes the Earth's elliptic properties. From here on, the steps ($n \to \infty$) describe smaller and smaller variations, until we get something like Figure 2.1. This is also the basic philosophy of the harmonic coefficients derived from GRACE data.
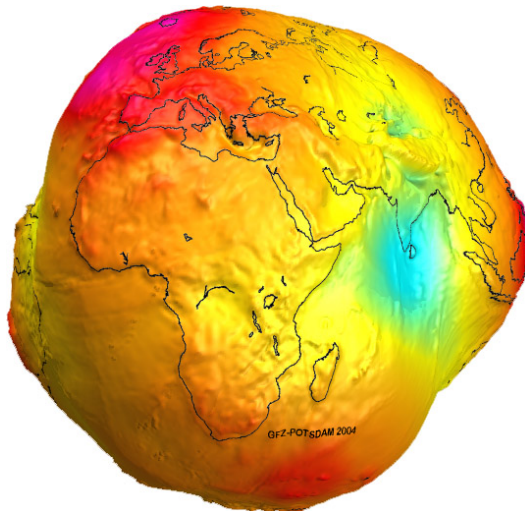
Figure 2.1: Exaggerated model of the geoid. Image courtesy of GFZ, Potsdam

This section is concluded by showing how one can compute the normalized Legendre Polynomials $\bar{P}_{lm}$ used throughout this thesis. The next section will look into how the GRACE satellites works, and how their data can be used in a way similar to that described in this section.

2.1.7 Legendre Polynomial

The normalized Legendre Polynomials $\bar{P}_{lm}$ used in this study are computed with the following procedure

$$
\begin{aligned}
\bar{P}_l(t) &= -\frac{\sqrt{2l+1}}{l}\frac{l-1}{\sqrt{2l-3}}\bar{P}_{l-2}(t)+ \\
&\quad t\frac{\sqrt{2l+1}}{l}\sqrt{2l-1}\bar{P}_{l-1}(t) & l \geq 2; m = 0 \\
\bar{P}_{ll}(t) &= \sqrt{\frac{2l+1}{2l}}\sqrt{1-t^2}\bar{P}_{l-1,l-1}(t) & l \geq 2; m = l \\
\bar{P}_{l,l-1}(t) &= t\sqrt{2l+1}\bar{P}_{l-1,l-1}(t) & l \geq 1; m = l-1 \\
\bar{P}_{lm}(t) &= -\sqrt{\frac{(2l+1)(l+m-1)(l-m-1)}{(2l-3)(l+m)(l-m)}}\bar{P}_{l-2,m}(t)+ \\
&\quad t\sqrt{\frac{(2l+1)(2l-1)}{(l+m)(l-m)}}\bar{P}_{l-1,m}(t) & l \geq 3; 1 \leq m \leq l-2
\end{aligned}
\tag{2.19}
$$

where $t = \sin\phi$. Since this is a recursive function, some initial values are needed. The first iterations of this function are listed in Table 2.1.

Table 2.1: The first iterations of the normalized Legendre Polynomials

l	m	$\bar{P}_{lm}(t)$
0	0	1
1	0	$t\sqrt{3}$
1	1	$\sqrt{1-t^2}$

2.1.8 Truncation of high frequencies

Higher frequency coefficients carry more noise and require substantially more computing time. Therefore, short wavelength signal is usually truncated at some point. Generally, the relation between the resolution in the area of study and the degree of coefficients one should use can be described as

$$
l_{max} = \frac{180°}{O°}
\tag{2.20}
$$

where $O°$ is the resolution with which one solves 2.28. This assumption is based on the Nyquist theorem and the degree and order of this thesis will be described in section 3.4 on page 30. For other purposes, one can wish to extend the frequency range substantially. The latest EGM geoid is for instance computed up to a degree and order of 2160, where the high frequency coefficients come from airborne and terrestrial gravimetric measurements [22]. The monthly GRACE data is published with a degree and order of 60 or 90. The GGM(s) geoids, which are purely based on GRACE data, are computed to degree and order 180.

2.2 GRACE

The data in this study is gathered from the Gravity Recovery and Climate Experiment (GRACE) twin satellites, launched in 2002. The satellites are the first of their kind, although after realizing their success and wide array of applications, more missions have been planned. The satellites track the gravity pull from any given point on the Earth surface very accurately by measuring the distance between them as they pass areas with greater or lesser gravitational pull by using various high-precision instruments. This change in separation distance can be used to calculate the gravitational pull of that area. They orbit the earth at about 450-500 km with an inclination of 89.5°. This segment of space is called the low orbit [26]. By lowering the orbit, it is possible to increase the resolution of the measurements. Closer to the atmosphere, there is; however, more particles creating drag forces and wear on the satellites [14]. The GRACE mission planned lifetime was originally planned through 2007 [39]. This has been extended, and the mission is now expected to provide data until the successor GRACE Follow-On (FO) is scheduled for launch in 2016. Figure 2.2 on page 14 shows an illustration of the twin satellites. In reality, the distance between them is about 220 km.

The raw data is calculated monthly into fully normalized spherical harmonic coefficients. The coefficients C_{lm}, S_{lm} are normalized to degree and order l, m. Although more data is available for some Level 2 data providers,
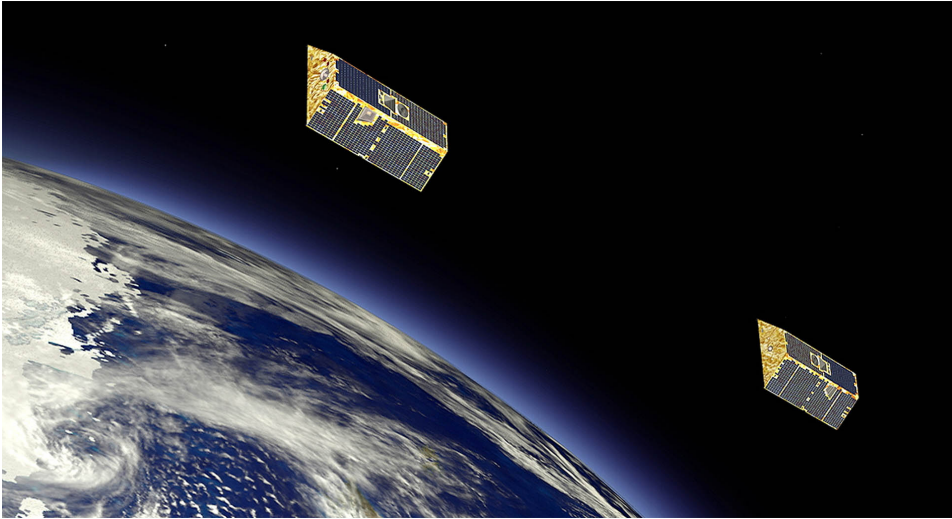
Figure 2.2: GRACE twin satellites. Image courtesy of GFZ, Potsdam

this report assess the results generated by order and degree 60 from three different institutes. These are JPL (Jet Propulsion Laboratory) at NASA, GFZ (GeoForschungsZentrum) in Potsdam and the CSR (Center for Space Research) at the University of Texas. The data has been filtered through the Wiener-type DDK5 used in RL05, a method developed by Kusche et al. [18].

The GRACE satellites have more applications than surveying the ice loss of Greenland. The accuracy of the measurements help oceanographers study ocean circulations due to a varying gravity field, hydrologists are able to monitor underground water reservoirs or map cycles in the great rivers. Solid Earth sciences can also benefit from the accuracy from the GRACE mission. For instance is it possible to estimate the post-glacial rebound [38], which directly influences the error correction of this thesis. Changes in the Earth's crust and lithosphere can also be tracked during or after earthquakes [21]. Combined, a collaboration of all these scientific fields aids us to a better understanding of the Earth's dynamic processes which in turn enables us to better predict the natural hazards and the human contribution to climate change.

In addition to the monthly solutions, the GRACE teams also publish geoid models, such as GGM02 and GGM03. These constitute the backbone of the very precise geoids such as the global EGM models [22] and the national models – for instance NMA2012v30 in Norway. These models use GRACE data for the long wavelength signals and increase the precision further with airborne and land based gravimetic measurements. Good geoid models are important keys to unlocking the full potential of many Earth sciences.

2.3 Description of the three GRACE data levels

The raw data from GRACE is handled by the three institutes JPL, GFZ and CSR. These institutes publish their monthly solutions through Physical Oceanography, Distributed Active Archive Center (PO.DAAC) located at JPL and Information Systems and Data Center (ISDC) at GFZ [4]. Figure 2.3 shows the data flow until it is finally ready in the bottom-right corner as monthly Level 2 data. In this section, we will take a quick look at how the data is transformed from raw satellite signal into useful monthly spherical harmonics.

2.3.1 GRACE Level 0 data

The first step in receiving GRACE data, is the raw satellite signal that is transmitted two times per day. This signal is extracted by JPL, GFZ and CSR. This signal includes navigational data such as GPS information, temperature readings and fuel usage in addition to the scientific measurements. The scientific data consists of distance measurements between the satellites, accelerometer data and positioning information [16].
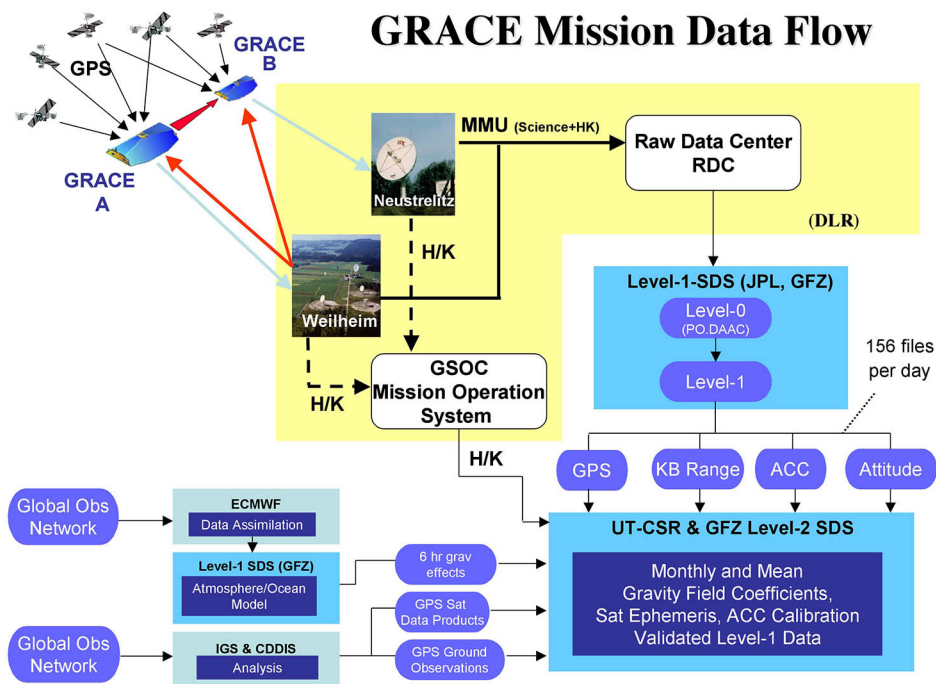
Figure 2.3: GRACE data flow. From raw satellite signal to Level 2 data. Image courtesy of CSR, Texas

2.3.2 GRACE Level 1 data

The next step is preprocessing and timestamping the data. This includes calculating and adding data from the K-band ranging system (measuring the distance between the satellites), the accelerometer and the navigation instruments; the GPS receivers and the star camera from both satellites [16]. From here, the Level 1 data is divided into an A and a B version, where the former is stored non-destructively and used for archiving, while the latter is more user-friendly, possibly irreversible, and used for publishing [4].

2.3.3 GRACE Level 2 data

The data that is used in this project, and most of the other scientific work based on GRACE measurements, utilizes Level 2 data. These are the monthly solutions that are released after validation of Level 1 data. The solutions from Level 1 are calibrated with precise orbit information and various terrestrial ancillary data [16]. These calibrations are done individually by the three institutes, although JPL's solutions are mainly meant for verification [16]. With the publication of the final Level 2 data sets, it is now time to compute the mass change using these measurements.

2.4   Modelling of mass change using GRACE data

In this section, we will see how the mathematical foundation laid in section 2.1 can be used on the data provided by GRACE, or more precisely the three institutes JPL, GFZ and CSR. Note that from this section, the general terms $\bar{A}_{lm}$ and $\bar{B}_{lm}$ are substituted with the terms C_{lm} and S_{lm}, which are commonly used by the providers of the data. We start by assuming that mass changes can be considered as a thin layer of water on the surface with varying thickness [17]. Even if the actual difference in height is bigger when ice is lost, it is convenient to compare it to fresh water, which has a consistent density. The loss of equivalent water height will reduce the gravitational pull in the areas where ice is lost, and hence the geoid formula (eq. 2.18 is useful. In his formula, one can substitute $N(r, \phi, \lambda)$ by $\Delta N(r, \phi, \lambda)$ if one also substitutes C_{lm} and S_{lm} by ΔC_{lm} and ΔS_{lm} respectively. Now, we suppose that the change was caused by a change in density distribution $\Delta \rho(r, \phi, \lambda)$. By the method of Wahr et al. [37] we can now define $\Delta \sigma$ as surface density, meaning that we integrate the density $\Delta \rho$ over a thin layer with thickness H

$$\Delta \sigma(\phi, \lambda) = \int_{\text{thin layer}} \Delta \rho(r, \phi, \lambda) dr \qquad (2.21)$$

17

This enables us to separate the contribution of the coefficients to a surface component and one solid Earth component

$$\begin{Bmatrix} \Delta C_{lm} \\ \Delta S_{lm} \end{Bmatrix} = \begin{Bmatrix} \Delta C_{lm} \\ \Delta S_{lm} \end{Bmatrix}_{\text{surf mass}} + \begin{Bmatrix} \Delta C_{lm} \\ \Delta S_{lm} \end{Bmatrix}_{\text{solid earth}} \qquad (2.22)$$

As long as H is thin enough and the wavelength ($l_{\max} = 60$) is small enough to satisfy $(l_{\max} + 2)H/a \ll 1$ we have for the two components of eq. 2.22

$$\begin{Bmatrix} \Delta C_{lm} \\ \Delta S_{lm} \end{Bmatrix}_{\text{surf}} = \frac{3}{4\pi a \rho_{\text{ave}}(2l+1)} \int \Delta\sigma(\phi,\lambda)\bar{P}_{lm}(\cos\lambda) \begin{Bmatrix} \cos(m\phi) \\ \sin(m\phi) \end{Bmatrix} \sin\lambda\, d\lambda\, d\phi$$

$$(2.23)$$

and

$$\begin{Bmatrix} \Delta C_{lm} \\ \Delta S_{lm} \end{Bmatrix}_{\text{solid}} = \frac{3k_l}{4\pi a \rho_{\text{ave}}(2l+1)} \int \Delta\sigma(\phi,\lambda)\bar{P}_{lm}(\cos\lambda) \begin{Bmatrix} \cos(m\phi) \\ \sin(m\phi) \end{Bmatrix} \sin\lambda\, d\lambda\, d\phi$$

$$(2.24)$$

In eq. 2.24, k_l denotes the Love number of degree l [37]. The Earth major semi axis is denoted by a and ρ_{ave} represents the average density of the Earth. These equations can be combined to express $\Delta\sigma$

$$\Delta\sigma(\phi,\lambda) = a\rho_w \sum_{l=0}^{\infty} \sum_{m=0}^{l} \bar{P}_{lm}(\sin\phi)[\Delta\hat{C}_{lm}\cos m\lambda + \Delta\hat{S}_{lm}\sin m\lambda] \qquad (2.25)$$

in which the density of water ρ_w is 1000 kg/m^3. To show the relationship between $\Delta\hat{C}_{lm}$, $\Delta\hat{S}_{lm}$ and ΔC_{lm}, ΔS_{lm}, we express eq. 2.25 in terms of $\Delta\hat{C}_{lm}$ and $\Delta\hat{S}_{lm}$

$$\begin{Bmatrix} \Delta\hat{C}_{lm} \\ \Delta\hat{S}_{lm} \end{Bmatrix} = \frac{1}{4\pi\rho_w} \int_0^{2\pi} d\phi \int_0^{\pi} \sin\lambda\, d\lambda\, \Delta\sigma(\phi,\lambda)\bar{P}_{lm}(\cos\lambda) \begin{Bmatrix} \cos(m\phi) \\ \sin(m\phi) \end{Bmatrix}$$

$$(2.26)$$

18

and finally, by combining eqs. 2.23, 2.24, 2.22 and 2.26 we get the relationship
we seek

$$\begin{Bmatrix} \Delta \hat{C}_{lm} \\ \Delta \hat{S}_{lm} \end{Bmatrix} = \frac{\rho_{\text{ave}}}{3\rho_w} \frac{2l+1}{1+k_l} \begin{Bmatrix} \Delta C_{lm} \\ \Delta S_{lm} \end{Bmatrix} \tag{2.27}$$

This is a useful relationship indeed, as ΔC_{lm} and ΔS_{lm} are the data provided
by GRACE. We can now finally arrive at an expression of $\Delta \sigma$ that is solvable
with GRACE data. Combining eqs. 2.25 and 2.27 we get

$$\Delta\sigma(\phi, \lambda) = \frac{a\rho_{ave}}{3} \sum_{l=0}^{\infty} \sum_{m=0}^{l} \frac{2l+1}{1+k_l} \bar{P}_{lm}(\sin\phi)[\Delta C_{lm}\cos m\lambda + \Delta S_{lm}\sin m\lambda]$$

$$\tag{2.28}$$

where ϕ and λ are the latitude and longitude of a point. ΔC_{lm} and ΔS_{lm}
are the monthly coefficients provided by GRACE. Note that one can divide
$\Delta\sigma$ [Δkg/m²] by the density of water ρ_w [kg/m³] and get the length unit [m].
This will correspond to the difference in height of water, i.e. a measure of
how much water has been lost or gained at the point of interest.

2.5   Computing the secular trend

To estimate the annual mass change and periodic variations in the monthly
anomalies, the following expression has been used [17]

$$f(\phi, \lambda, t) = A + Bt + \sum_i C_i \cos(\omega_i t) + D_i \sin(\omega_i t) + \epsilon \tag{2.29}$$

in which the value f represents ice mass anomaly at the location (ϕ, λ) at the
time t. In this expression, A represents a static value. The first-order variable
B describes the secular component. The periodic fluctuations are expressed
with the frequencies ω_i and amplitudes C_i and D_i. The last variable, ϵ
describes noise. The periodic fluctuation component in this equation is

equivalent to one month, and the secular component takes the entire period of 2003–2012 into account.

2.6 Corrections

This project uses mainly two kinds of corrections additional to the corrections made by JPL, GFZ and CSR on the Release 05 data (RL05). The most important one is the gravity leakage and the second is the post-glacial rebound. In this section, both will be described thoroughly. Additionally, we will look into the improvements in GRACE RL05, and discuss the replacement of coefficient representing the Earth's dynamic oblateness. We also take a quick look at the non-isotropic smoothing used in the latest releases of Level 2 data.

2.6.1 Gravity leakage

The gravity leakage effect pollutes the computations by (1) propagation of signal from the areas around Greenland (leakage in) and oppositely by (2) the depletion of signal from Greenland out to the same areas (leakage out). These effects does not cancel each other out and needs to be assessed separately [17]. It is assumed that the leakage effect from GRACE RL05 data should be smaller than previous iterations, as the effect comes from limited spatial resolution and imperfect reduction of satellite measurements errors, such as system-noise, oscillator error and small orbit misinformation [31]. Since gravity signal flows in three dimensions, its effect diminishes quickly. Theoretically, one should take into account the effect on the entire planet, but because of this rapid decay in magnitude, it is sufficient to calculate the effect in the immediate area around Greenland [3]. Omitting the leakage effect has been showed to increase the mass loss effect on Greenland by up to a factor 2 [3]. The method for computing the leakage effect can be interpreted as removing the surplus signal and adding the escaping signal. The two procedures are mainly identical, with the difference being whether

one starts with values from the inside of Greenland or outside of Greenland. The two procedures can be described as following

Leakage out Firstly, one calculates a preliminary set of values of the mass change on Greenland using the global spherical harmonic coefficients. Secondly, one reverses this process to create a new set of spherical harmonic coefficients based on these values. Thirdly one uses these new coefficients (containing only local information plus leaked signal) to calculate a mass change over the entire area within which one wants to assess the leakage effect. Fourthly one calculates yet another set of spherical harmonic coefficients based on this area, and lastly, one uses these coefficients to calculate the mass change inside Greenland. The result will reflect the gravity signal that has been propagated into Greenland from the surrounding land masses.

Leakage in This procedure is very similar to the method above, but instead of starting with a preliminary set of values of mass change on Greenland, one starts by calculating the mass change outside the area of interest, i.e. the entire northern cap of the world except Greenland.

2.6.2 Post-glacial rebound effects

Also called Glacial Isostatic Adjustment (GIA), this is an effect where one can observe an uplift in areas that were covered by an ice cap during the last ice age. The effect is caused by the residual tension in the crust left by the melted snow and ice. The high viscosity of the Earth's crust and upper mantle makes this a slow process, still discernible today [23]. The process of the post-glacial rebound causes variations in the gravity field and these variations are detected by GRACE. It is possible to model the effect and then subtract the expected effect from the GRACE data, but it has been proved to be difficult to predict this effect accurately. The three main challenges in creating a good PGR model are (1) determining how the ice used to be distributed, (2) assessing the viscosity of the mantle and (3) estimating a physical and mathematical model [16].

There has been some controversy on whether one should correct for the post-glacial rebound effect. Guo et al. suggest in a comparison of 14 PGR models that new and better models need to be worked out to fully exploit the potential of GRACE data [13]. Baur et al. chose not to include PGR corrections in their assessment of the gravity leakage issue due to the large error bounds considered with the proposed solutions [3]. Velicogna and Wahr on the other hand, chose to apply the corrections provided through the ICE-5G model [34]. This model uses the VM2 viscosity profile [11]. NASA estimates the uncertainty of this model to be about $\pm$ 20 %, based on comparing different viscosity values. This means that the correction itself probably is greater than the uncertainty of the correction.

2.6.3 Different GRACE releases

In this project, the Release 05 models from GRACE have been used. Compared to Release 04 (RL04), the biggest differences are (i) reduced north/south stripes and (ii) reduced east/west banded errors [5]. This has been achieved through a better insight into the alignment between the star camera, the onboard accelerometer and the K-band ranging system for Level-1B data in addition to a an updated gravity field, tidal effects and better de-aliasing for Level-2 models [6]. Also worth mentioning is that the secular rates in Release 04 had empirical values for C_{20}, C_{30}, C_{40}, C_{21} and S_{21} while no such rates have been used in Release 05. The quality of C_{20} for all the three models (JPL, CSR and GFZ) will be examined in this report. The practical consequence of this is that the science data centers provides models that are more consistent among themselves, and better estimation of uncertainty [6]. Release 05 was published during the first months of 2013.

2.6.4 Considering replacement of coefficients for Earth's dynamic oblateness

The coefficient C_{20} represents the flattening of the Earth and is usually called the Earth's dynamic oblateness [8]. According to satellite laser ranging (SLR),

this value has been indicated to vary during the years of measurements. The secular trend is a decrease of about $-2.75 \times 10^{-11} \mathrm{yr}^{-1}$ with additional seasonal variations. In the iterations of GRACE up until now, the values of C_{20} would generally have to be substituted with values from the SLR measurement table. This project assesses the difference between SLR data and contemporary GRACE satellite data for the C_{20} values, as GFZ now recommend not substituting these values, while both CSR and JPL recommend substitution. If the satellite values are found to be good enough, they will not be substituted in this project.

2.6.5 Non-isotropic smoothing

Correlated and resolution-dependent noise in the harmonic coefficients provided by the monthly gravity field solutions are problems that need correction. These problems are most prominent in the higher harmonic frequencies, but truncating the solutions at a resolution low enough to avoid the problems causes the loss of too much significant signal [18]. Thus, it has to be dealt with in some other way. This noise has become known has the "striping" effect. Figure 2.4 show the striping effect and the solution to the problem with smoothing and correlated-error filters [30]. The stripes shown in the figure indicates a correlation in the gravity field coefficients. Note that the smoothing radii in Figure 2.4 are different than the DDK filter radii used in the latest GRACE Level 2 releases.

Earlier, the solution to the striping problem seen in Figure 2.4(a) was Gaussian smoothing [37]. The philosophy is based on convolving the higher frequencies against an *isotropic* Gaussian smoothing kernel. This was proposed in 1998. Swenson and Wahr refined this method in 2002 [29] and later, they designed a *non-isotropic* kernel that has proved to yield better results [30]. Here, Gaussian smoothing is applied after decorrelation. The GRACE Level 2 solutions in the latest release (05) have been processed through the DDK1–DDK5 filters [18]. Table 2.2 shows the smoothing radius used in the three first decorrelation filters. For the two latest filters, DDK4 and DDK5, no smoothing radius information has been provided by Kusche or others.

Isotropic or non-isotropic filtering is applied before publication and is thus not something the author of this study has done. Still, it is a crucial part of the error correction, and therefore mentioned here. Finally, note that the coefficients go through several smoothing steps with different radii. The reason for this is eliminating striping that appear at different frequencies.
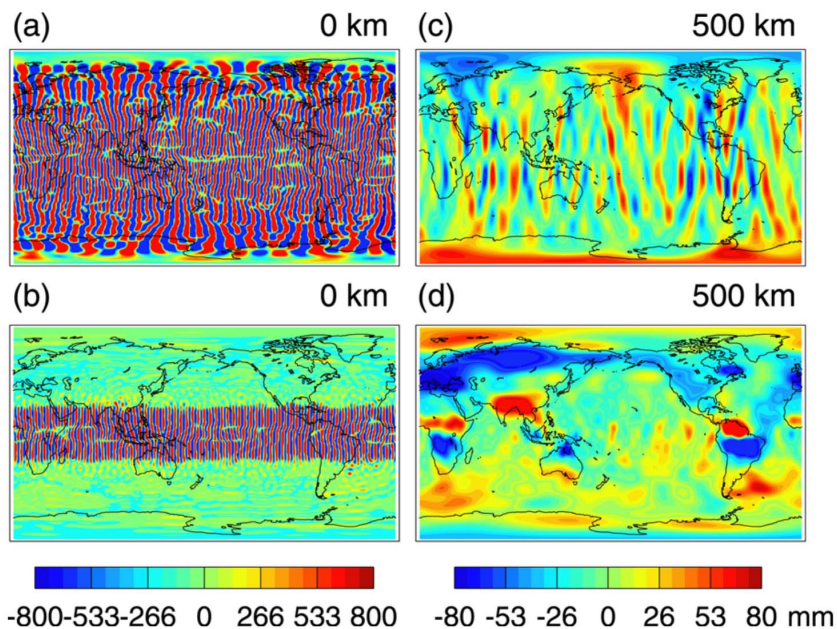
Figure 2.4: GRACE-derived maps of monthly anomaly of water storage. (a) Unfiltered, no smoothing; (b) filtered with correlated-error filter, no smoothing; (c) unfiltered and smoothed with 500 km Gaussian; (d) filtered with correlated-error filter and smoothed with 500 km Gaussian. Image courtesy of Geophysical Research Letters [30]

Table 2.2: Smoothing radius in the DDK1–3 decorrelation filters [18]

Filter	Radius km
DDK1	1350
DDK2	900
DDK3	660

Chapter 3

Methodology

In this chapter, an elaborate description of the procedure is given. In section 3.1, all software used in the computations is described. In section 3.2, additional software is described for correcting gravity leakage and post-glacial rebound. Furthermore, in section 3.2.3, it is explained how gaps in the GRACE data sets were handled and in section 3.3, the hardware used for the computations is briefly described. In section 3.4, the choice of resolution is described. The last two sections in this chapter deals with describing the computation of the area of Greenland and how the results are finally plotted.

3.1   Programming and procedure

The main component of this project has been computation or reverse-computation of spherical harmonics. Additionally, quite a few other small programs were used to different tasks. Much of the software used in this project has been generously provided by Gholamreza Joodaki at NTNU. Some of the software has been written specifically for this project. In this section, a very brief presentation will be given on how the programs work and then how they are batched together to include the corrections. All software is written in Matlab R2010b and GMT 4.5.6.

3.1.1 Selecting coordinates

First of, it is practical to set up lists of the coordinate pairs needed for the task ahead. For this project, a resolution of $0.5°$ was chosen for the Greenland island, while computations outside Greenland were set to a resolution of $1.0°$. In Matlab, there is a built-in shapefile with a decent quality for all the land areas of the world. Using this, one can extract the bounding polygon, create a rectangle with a $0.5°$ mesh of coordinates covering this polygon and finally use Matlabs *inpolygon* method to select only coordinates inside the Greenland shape. Similarly, a grid of coordinates for the entire northern cap ($\phi \geq 60°$) of the world is produced with a resolution of $1.0°$. For simplifying things later, this grid also contains the coordinates on Greenland, although a third column (in addition to a λ and a ϕ column) is added with value 1 if the coordinate pair is on Greenland and 0 elsewhere.

3.1.2 Sort coefficients and compute averages

For all computations based on the harmonic coefficients, it is favorable to sort the coefficients. This was done in a way shown in Figure 3.1. After this, all currently relevant matrices (one for each month in the period of interest) for a given model were loaded and an average matrix was calculated. This is useful for computing secular trends.

$$
\begin{array}{ccccccccc}
 & & & & C_{0,0} & & & & \\
 & & & C_{1,1} & C_{1,0} & S_{1,1} & & & \\
 & & C_{2,2} & C_{2,1} & C_{2,0} & S_{2,1} & S_{2,2} & & \\
 & \iddots & \vdots & \vdots & \vdots & \vdots & \vdots & \ddots & \\
C_{60,60} & \cdots & \cdots & \cdots & \cdots & \cdots & \cdots & \cdots & S_{60,60}
\end{array}
$$

Figure 3.1: Structure of organized spherical coefficients coefficients in Matlab

3.1.3 Density computation

In this program, a loop is set up for each of the monthly coefficient matrices; 114 or 115, depending on which model is considered. This program computes eq. 2.28. In the end, this program prints a file for each of the points inside Greenland containing the months and their corresponding $\Delta\sigma$.

3.1.4 Secular trend

The next program loads all the files exported from the previous program and calculates the secular trend for all the points over all the months. The program can also be configured to only calculate an excerpt, for instance for plotting the trend in a shorter period of time.

3.1.5 Methods used in GMT

With the data from the trend program, it is now possible to plot the preliminary results, to see if they are consistent with previously published data. This was done using various scripts written in the Generic Mapping Tools (GMT) environment. Using GMT meant another steep learning curve, as this system was completely new for the author of this study before the project started. The GMT scripts uses a range of different methods, the most used ones for this project are listed and briefly explained here:

makecpt defines the color scheme and the contour line intervals
psbasemap initiates the background map
gmtselect loads the land area polygons
grdlandmask masks out Greenland
grd2xyz transforms the land mask from a grid to a list of coordinates
psmask creates and draws a new land mask for Greenland to the output
nearneighbor defines the interpolation technique between the points
grdimage draws land grid to the output file
grdcontour draws the contour lines to the output file
pscoast draws the coast lines to the output file

3.2 Corrections

After verifying the preliminary results from the computations described above, it is time to extend the programs to also consider corrections for post-glacial rebound and gravity leakage effects. This was achieved using the same software, with slight modifications to the code. The steps are described in the following subsections.

3.2.1 Post-glacial rebound

The first (and least time consuming) correction is that of the post-glacial rebound. To calculate this, an external file containing the ICE-5G coefficients [23] was loaded into the program described in section 3.1.3. The corrections are in the form of spherical harmonic coefficients. An average value over the number of months in the study was calculated, and this mean was subtracted from the coefficients provided by GRACE. Another computation, only plotting the coefficients from the post-glacial rebound data file was also conducted. The result allow us to see the magnitude of the effect in the period of interest. The result is presented in section 4.2 on page 37.

3.2.2 Gravity leakage

This effect was calculated independently of the initial computations and requires a few extra steps. It consists of two sub-computations – one considering the leakage out effect and the other considering the leakage in effect. For the leakage out, the preliminary results from the program described in section 3.1.3 were loaded. These contain values of $\Delta\sigma$ inside Greenland. Based on these data, one can calculate new global spherical harmonic coefficients by reverse-computing eq. 2.28 described on page 19. The next step now is to calculate $\Delta\sigma$ for the entire northern cap of the world, ($\phi > 60°$). To save (several weeks of) computing time, this was done on a 1° degree resolution, instead of the 0.5° resolution used inside Greenland.

One would perhaps assume that this step would produce something similar to the preliminary data where the information on Greenland would be unaltered and the values outside Greenland would all be zeroes. However, this is not the case due to the leakage effect. The process is now repeated on the new data set for the entire northern cap: New spherical coefficients are computed, and based on these, one can compute a new value for $\Delta\sigma$ on the 0.5° resolution set of points on Greenland. The result will now reflect the equivalent water thickness of gravity signals leaking out of Greenland and thus be directly added to the preliminary results.

A similar case exists for the leakage in signals, and these must be subtracted to accurately assess the mass change in the period. The process is identical to that of computing leakage out, but in the first step, one would use another set of preliminary values, this time based on $\Delta\sigma$ computed for every point on the northern cap in a one degree grid outside of Greenland. In this way, one will identify the magnitude of gravity signal leaking into Greenland from the surrounding masses, most prominently Scandinavia and the north-eastern parts of Canada.

The results from the leakage effect are added or subtracted to produce the final results, and figures showing the effects are included in the results section on page 39.

3.2.3   Gaps in the GRACE data sets

At some of the months in the measurement period, the GRACE satellites had gaps in the solutions [36]. On these occasions, values from the surrounding months were used to linearly interpolate the missing data. As none of the gaps were consecutive for more than two months, this should not significantly affect the accuracy of the results in this thesis. For a complete overview of missing solutions, see Figure 2.4 on page 15 in the PhD thesis of Joodaki [16].

3.3   Hardware

The computations in this project were quite time-consuming. The estimated total of time on computations is about three weeks. The Matlab programs were written to utilize multiple CPU threads and the computations were performed simultaneously (where applicable) on two personal computers, one desktop and one laptop computer with the following processor specifications

Desktop i7-2600K (Sandy Bridge) @ Overclocked 4.20 GHz, 8 threads
Laptop i7-3517U (Ivy Bridge) @ Standard frequency 2.4 GHz, 4 threads

Additional specifications are omitted, as such elements as GPU (Graphics Processing Unit), RAM (Random Access Memory) and SSD (Solid State Drive) performances do not significantly affect computing time. The single most time-consuming project was computing the gravity leakage-in effect. Running on all accessible threads, the total computation time for this operation clocked in at over 250 hours. It is possible that some of the tasks could be parallelized to utilize the graphics processors of the machines, but further investigation was not done as many of the equations contain recursive components, and are hence difficult to parallelize.

3.4   Spatial resolution and frequency cutoff

The resolution for this project was chosen to be $0.5° \times 0.5°$ (2541 points) for the computations on Greenland and $1.0° \times 1.0°$ (10800 points) for the computations on the surrounding areas needed to study the gravity leakage effects. This area covers $-180° \leq \lambda < 180°$ and $60° \leq \phi \leq 90°$. Eq. 2.20 (based on the Nyquist Theorem) would the suggest using a maximum degree and order of

$$l_{max} = \frac{180°}{0.5°} = 360$$

for the high resolution areas on Greenland and

$$l_{max} = \frac{180°}{1.0°} = 180$$

for the lower-resolution areas on the rest of the northern cap of the planet. The monthly solutions are mostly provided to a degree and order of 90, yet in this project, a degree and order of 60 was chosen. This was mainly to save computation time. The time difference factor between degree 60 and 90 is

$$\frac{\sum_{n=1}^{91} n}{\sum_{n=1}^{61} n} \approx 2.2$$

and the accuracy gains of the increase from 60 to 90 were considered too small to justify a doubling of the computation time. The consequence of this decision is that the results will to a slightly greater degree reflect the long-wavelength information. This is probably acceptable since the area of study is big, even on a global scale. In some months, only a degree and order of 60 were available. Combining degree and order 60 somewhere and 90 other places would only contribute to a more difficult assessment of the random error in the computations.

3.5 Ice mass estimation

To estimate the total mass change for Greenland, one can multiply the difference in equivalent water height with the density of water and the area of interest. This section describes how this can be achieved. To calculate the area of Greenland, an integral approach in Matlab was chosen. This involves determining the area that the polygon of Greenland occupies on a unit sphere, and then multiplying by the surface are of the Earth. The first step then, is to calculate the area of the planet. The mean radius of the Earth was set to $6371\,\text{km}$, making the area of the Earth spheroid $4\pi 6371^2\,\text{km}^2$ $= 5.101 \cdot 10^8\,\text{km}^2$. The area of Greenland was computed in Matlab using the *areaint* method, which is an integral technique to calculate a spherical surface fraction area. The input to this function is the polygon surrounding the points in this task and the output multiplied with the area of the Earth spheroid is $2.055 \cdot 10^6\,\text{km}^2$.

The unit of eq. 2.28 is cm, and this corresponds to a change in equivalent water height. It might be more interesting to talk about the total mass change for the entire island, and this can be done by multiplying $\Delta\sigma$ with the density of water $^{kg}/m^3$ and the total area m^2. This unit will be $^{kg\ m^3}/m^3$. The distance units cancel out after converting them to the same scale, and the final unit is kg. The conversion rate then makes $1\,cm \mapsto 20.55\,Gigaton$. This, of course, assumes $1\,cm$ over the entire island. The different coordinates yields different variations, but one can now calculate the average $\Delta\sigma$ over the total area and simply multiply by 20.55 to get the mass change in Gigaton. This can be done monthly so that one can do a regression analysis and thus find the slope of the mass change. These results are presented in section 4.4 on page 42.

3.6   Error estimation

In this project, systematic and random error has been assessed separately and added for a total error estimation. Systematic error has been computed with the following formula

$$E_{\text{systematic}} = \sqrt{\sum_{i=1}^{n} \left(C_{0i}^2 + C_{1i}^2\right)} \tag{3.1}$$

where we sum for all the n coordinates over which the error is estimated. C_0 denotes the results from the computation of the uncorrected values. Hence, this error estimation has been done individually for all the three models C (JPL, GFZ and CSR). C_1 denotes the same models corrected for gravity leakage and post-glacial rebound. Random error accounts for about $^1/_{10}$th of the total error and has been computed using the following formula

$$\sigma_N(l) = a \sqrt{\sum_{m=0}^{l} \left(\sigma_{C_{lm}}^2 + \sigma_{S_{lm}}^2\right)} \tag{3.2}$$

where $\sigma^2_{C_{lm}}$ and $\sigma^2_{S_{lm}}$ are the errors on the gravity potential coefficients and a is the radius of the Earth [16]. The letter l represents the degree at which the computation is performed and should reflect the degree and order of the computations on the actual coefficients. The formula corresponds to the square root of the variance of the error coefficients attached to the monthly GRACE solutions. Note that CSR has not provided any error coefficients and is therefore not included in the error estimation. Since the main contribution to the error is systematic, this does not critically affect the error estimation.

3.7 Plotting the results

The figures in this thesis were generated by scripts written for Generic Mapping Tools (GMT). An introduction to this environment were given by my mentor Joodaki Gholamreza. In addition, he also provided me with scripts he had already used himself on similar visualization tasks. Only a few code changes were then needed to present the findings of this project while at the same time a very useful skill was gained in the process. Graphs are presented directly from data files using the TikZ package in LaTeX. Using this package involved learning another useful skill.

Chapter 4

Numerical investigation

This chapter will present and comment the results of the computations. The first section shows the differences between the values of the Earth's dynamic oblateness. Section 4.2 presents the model of post-glacial rebound used in this thesis. Section 4.3 shows the results for the gravity leakage effects in the polar region, while section 4.4 presents figures showing the extent of the ice mass loss on Greenland. Three separate models are displayed for both JPL, GFZ and CSR. The plots are from the periods 2003–2007, 2003–2010 and 2003–2012. By also plotting the partial plots, it is possible to see the movement of the mass loss activity.

4.1 Earth's dynamic oblateness term estimation

This section describes the differences between the coefficient C_{20}; the Earth's dynamic oblateness in the various models and the values of C_{20} from satellite laser ranging (SLR) data provided through GRACE network. This coefficient can be interpreted as the flattening of the Earth, i.e. its ellipsoid properties. The figures in this section plot these differences for RL04 and RL05 for JPL, GFZ and CSR. Furthermore, the figures are commented directly underneath. For simplified comparison, the three figures have the same scales, even

though this means not all three models will use the full extent of their scales.

GFZ no longer recommends substitution of C_{20} in RL05, while both JPL and CSR does. The findings in this thesis are that the values of C_{20} from the models now are well within the values of tolerance. Especially the GFZ and CSR models have been significantly improved in RL05 over RL04. In the JPL model, the C_{20} values are furhter away from the SLR values in RL05 compared to RL04. The differences are; however, very small in all three models and it was chosen not to substitute any values of C_{20} for the computations in this project.

Figure 4.1 shows the plot of ΔC_{20} from SLR data versus JPL RL04 and RL05. For some reason, we observe a greater difference between GRACE data and satellite laser ranging in Release 05 than in Release 04. The difference is however well within our domain of acceptance.
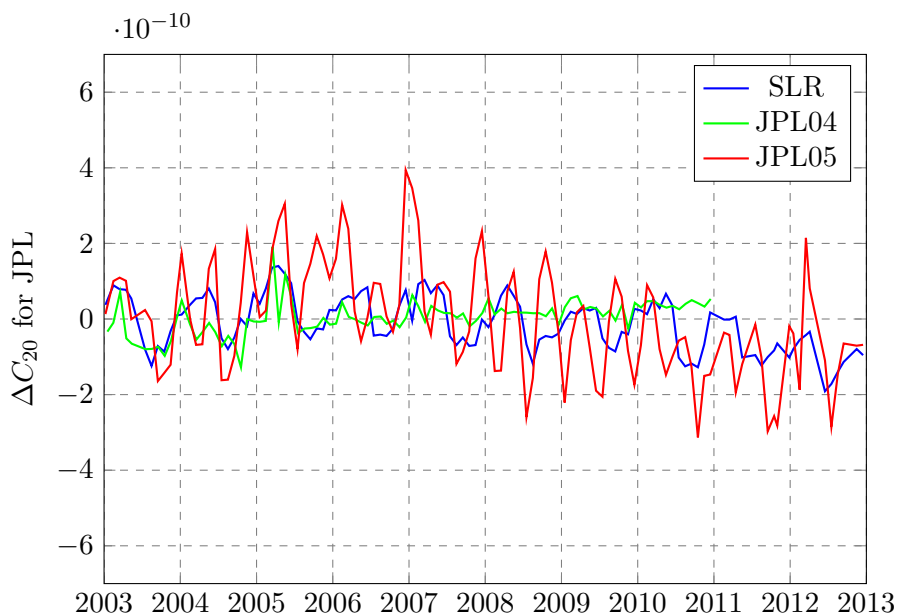

Figure 4.1: Comparison of ΔC_{20}-values from SLR versus JPL Release 04 and Release 05

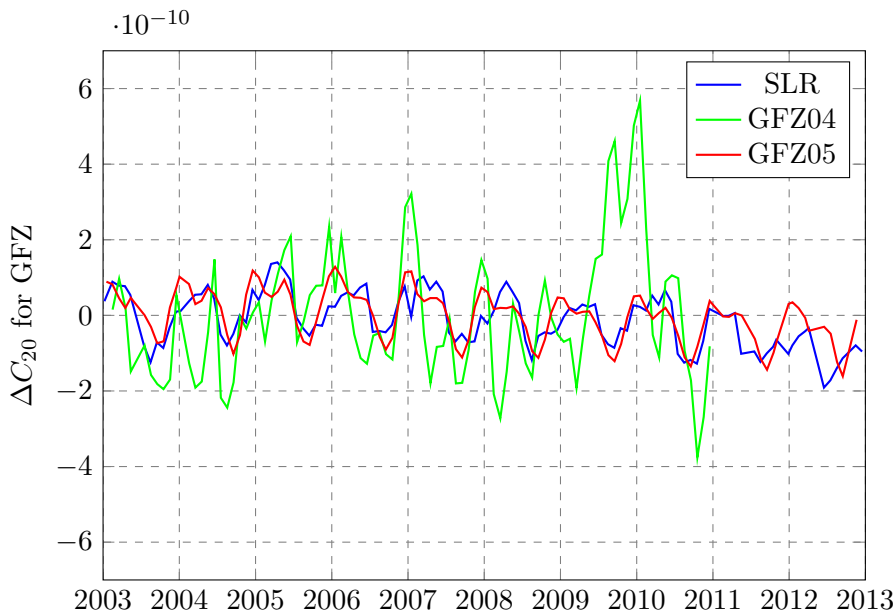Figure 4.2 shows a similar plot with GFZ data. Here, the difference between

Figure 4.2: Comparison of ΔC_{20}-values from SLR versus GFZ RL04 and RL05

GRACE data and satellite laser ranging is extremely little for GFZ's Release 05 compared to Release 04.

Lastly, Figure 4.3 on page 38 shows the same plot with CSR data. In some regions, the CSR's RL05 is not significantly better than their RL04 when comparing ΔC_{20} with satellite ranging data. In other periods – for instance all through 2010, it has become substantially better.

4.2 Post-glacial rebound

During the last ice age, a massive ice sheet covered the entire northern cap of the world. This created a great pressure that is still felt by the Earth crust in the region. Due to this, most northern parts of the world are experiencing an uplift, creating disturbances in gravity measurements [23]. This effect has been calculated and the results are presented in the same unit as the rest of the calculations of this project: cm/yr. Figure 4.4 illustrates these
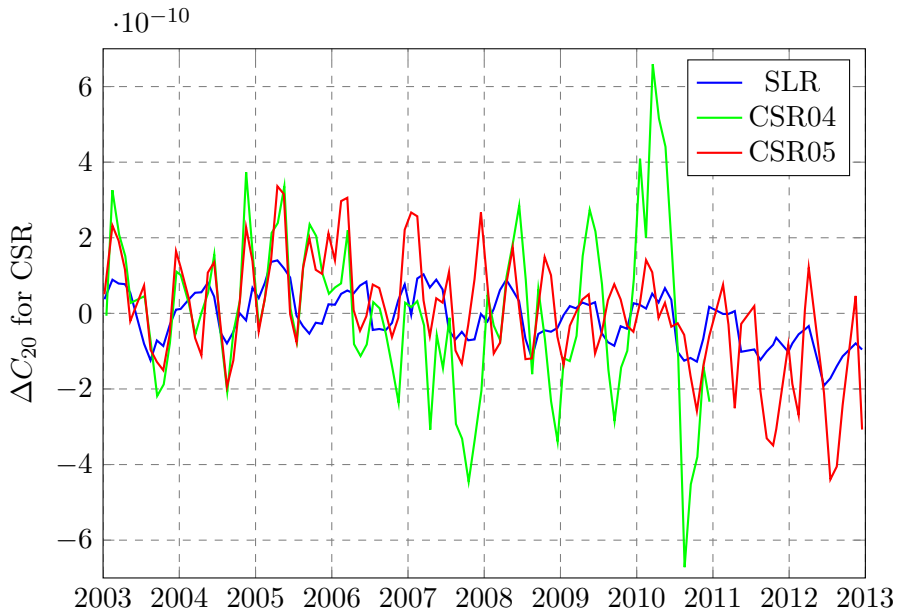
Figure 4.3: Comparison of ΔC_{20}-values from SLR versus CSR RL04 and RL05

results. These values have been directly subtracted from the final results presented in this thesis. Negative values on the scale corresponds to the inverse of the land rise. Because of this, the figure shows the values that needs to be added to the final results.

Correcting for the post-glacial rebound has been a topic of controversy. In this thesis, the accuracies of the available models have not been assessed, but it has been assumed that the effect of correction is greater than the standard deviation of the models. This assumption is supported by Velicogna and Wahr [34] and Joodaki [16]. The results vary from an annual 1.3 cm fall to 2.2 cm rise, with an average for Greenland of 0.14 cm/yr rise over the 10 year period that this project covers. This is, of course not a very big correction, but it adds a little precision to the final results.
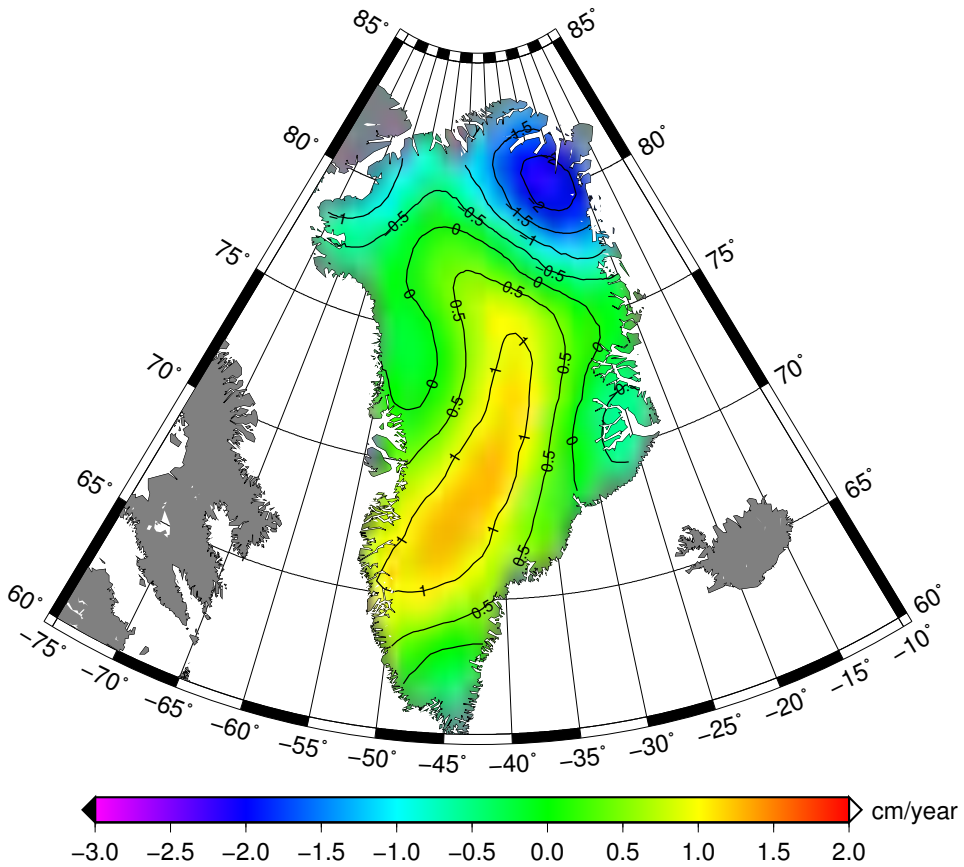
Figure 4.4: Effect of post-glacial rebound on Greenland

4.3 Gravity leakage effect

In this section, figures from the gravity leakage computation are presented. This is the correction with the greatest effect on the final results, on average contributing to an equivalent of approximately ± 10 Gigaton annually. The figures show an average effect from the three data sets (JPL, GFZ and CSR). In the final results, the gravity leakage effect has been considered individually for the data sets. The results show, in compliance with the study of Baur et. al [3], that the effect of the leakage out effect is greater than the leakage in effect.

Figure 4.5 shows how signal around the northern cap is diluted and leaking into Greenland, especially just inside of the coastline. Figure 4.6 shows how the gravity signal leaks out from Greenland, most notably immediately outside the cost.
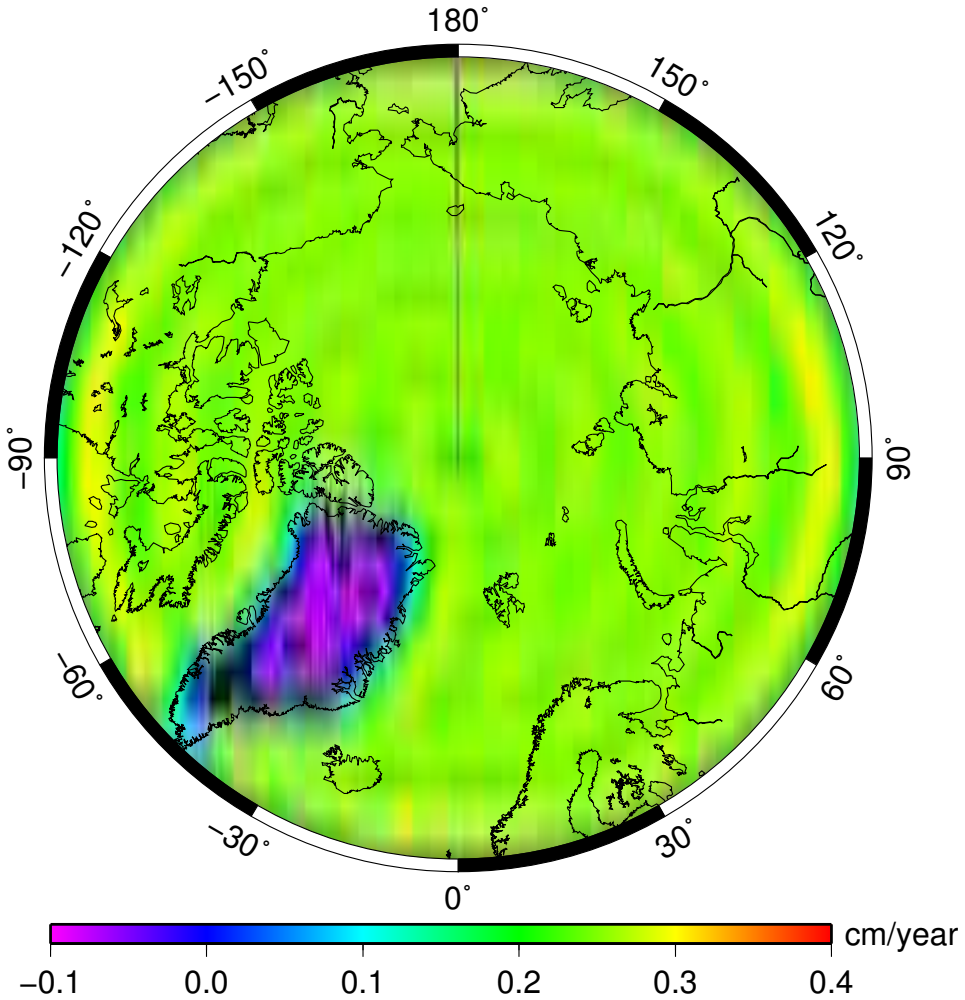

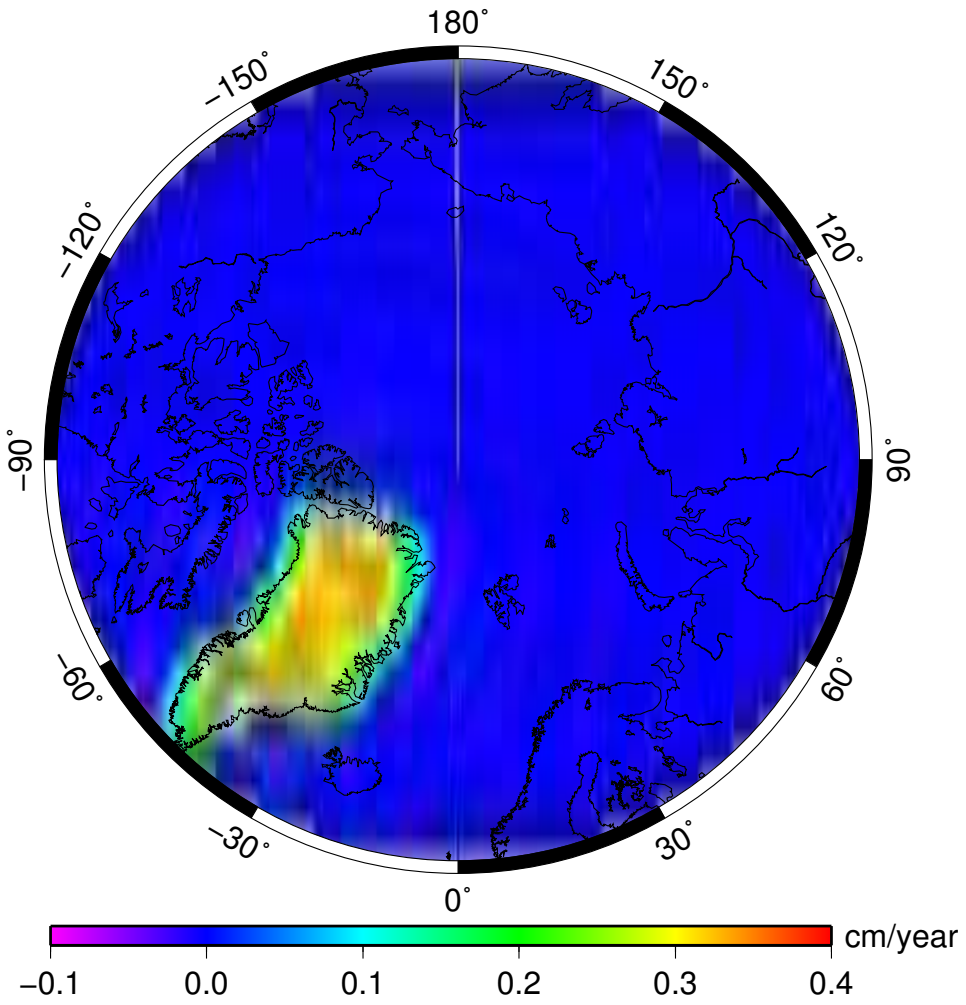Figure 4.5: Leakage in effect in the area around Greenland, $\phi \geq 60°$

Figure 4.6: Leakage out effect in the area around Greenland, $\phi \geq 60°$

4.4   Secular trend in the period 2003 through 2012

This section totally shows ten figures. For all three contributors of Level 2-data (JPL, GFZ and CSR), three plots are specified. One with data from 2003–2007, one with data from 2003–2010 and one with data from the entire period, 2003–2012. This enables us to track the change with which the ice mass loss is moving over Greenland. For simplified comparison, all the figures have the same scale. This means that not all models will use the full extent of the scale, but enables us to compare the different figures directly. Originally, the following figures had contour lines (like, for instance Figure 4.4 on page 39, but these have been removed as we are generally not interested in where the contours are, but more so to see the movement of the ice mass change over time.

The last figure is a graph showing the secular trend over the entire period. Also included is a table showing the minimum and maximum values from all the models. See Table 4.3 on page 57. Note that the global minimums and maximums in Table 4.3 are in bold typeface. These values were used to specify the scale range in Figures 4.7–4.15. The "Min" values corresponds to the greatest annual ice loss in cm/yr and the "Max" values corresponds to the greatest annual ice gain in cm/yr. The figures 4.7–4.15 can be interpreted as spatial visualizations of the secular trend illustrated in Figure 4.17 on page 53.

4.4.1   Results from the JPL models

The first figure shows a plot of the mass balance based on the JPL RL05 model in the period 2003–2007. The scale is annual equivalent water depth change in cm. We see that the north-eastern parts of Greenland is gaining some ice during this period, while the south-east is losing ice, somewhere close to -24 cm/yr. There is also an area on the west coast around $\phi = 75°$ where there is a slightly higher ice loss than the main trend of the figure. Lastly, there is a small area on the south-west that is slightly gaining ice.
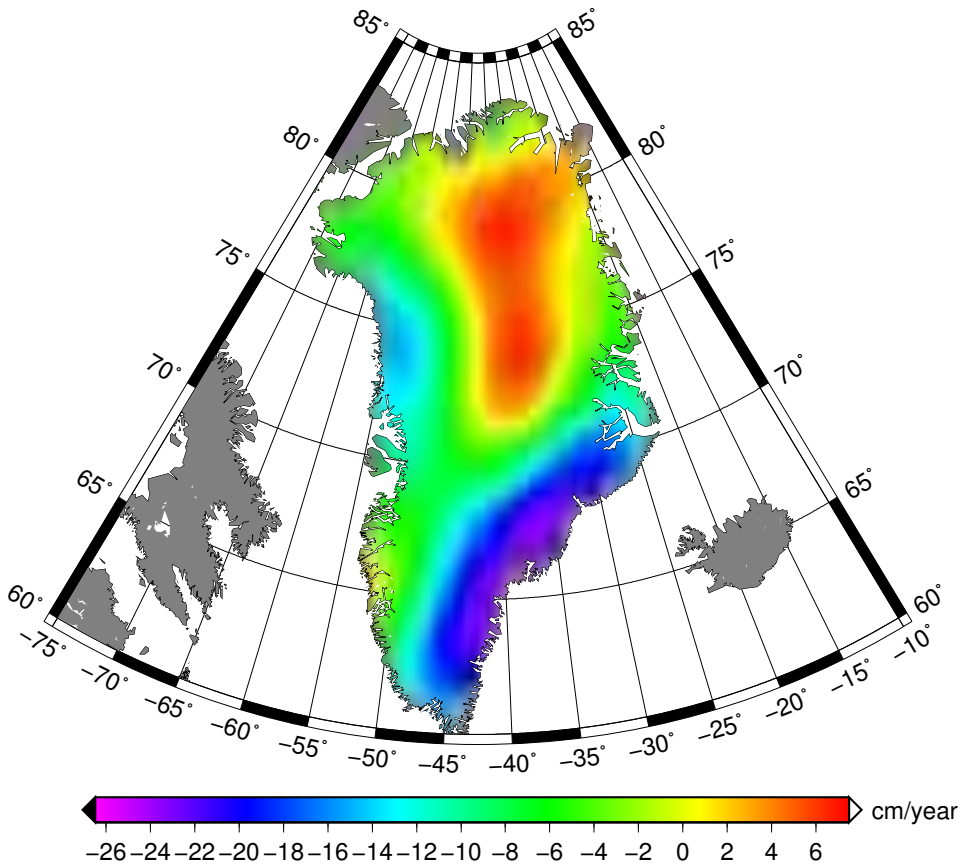
Figure 4.7: Greenland ice mass balance in the period 2003-2007 based on Level 2 GRACE data from JPL

When the computation for JPL is extended to include the period through 2010 (see Figure 4.8), we can notice some changes from the previous figure. Maybe the most obvious is that the blue area previously seen in the south east is now spreading towards the west and the slight ice gain we could see in the south-west is now also in decline. Also noticeable is the significant extension of the ice loss area in the west, at around $\phi = 75°$. The ice gain is also smaller in the north-east, and we now observe a loss all along the coast. At the same time, the most rapidly declining areas observed in the previous figure is not declining just as fast when the data is extended to 2010. This is prominent on the east coast, around $\phi = 65°$.
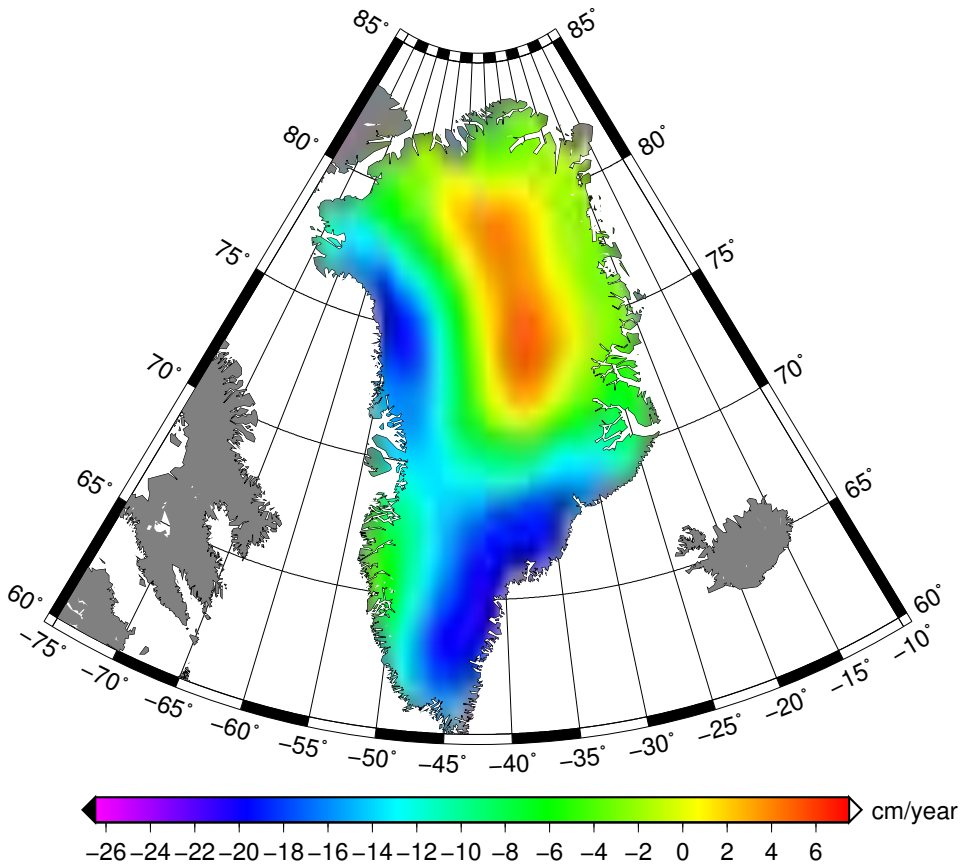
Figure 4.8: Greenland ice mass balance in the period 2003-2010 based on Level 2 GRACE data from JPL

When data from the entire period 2003-2012 is included, we can see from Figure 4.9 a continuation of the trend we observed when comparing data ranging through 2007 with data through 2010. The mass loss is continuing to spread to the west, and the areas in which the ice is increasing are still becoming smaller. In Figure 4.7, we could see purple areas in the south-east (ice loss $\geq 22\,\mathrm{cm/yr}$.) When the data through 2010 was included, this reduction had eased slightly, but it is now back again when we include data through 2012. It is now a continuous blue area from the far south-east up to the west coast at $\phi = 75°$. There is still a slight mass gain in the northern central parts of Greenland, but this area is clearly becoming smaller.
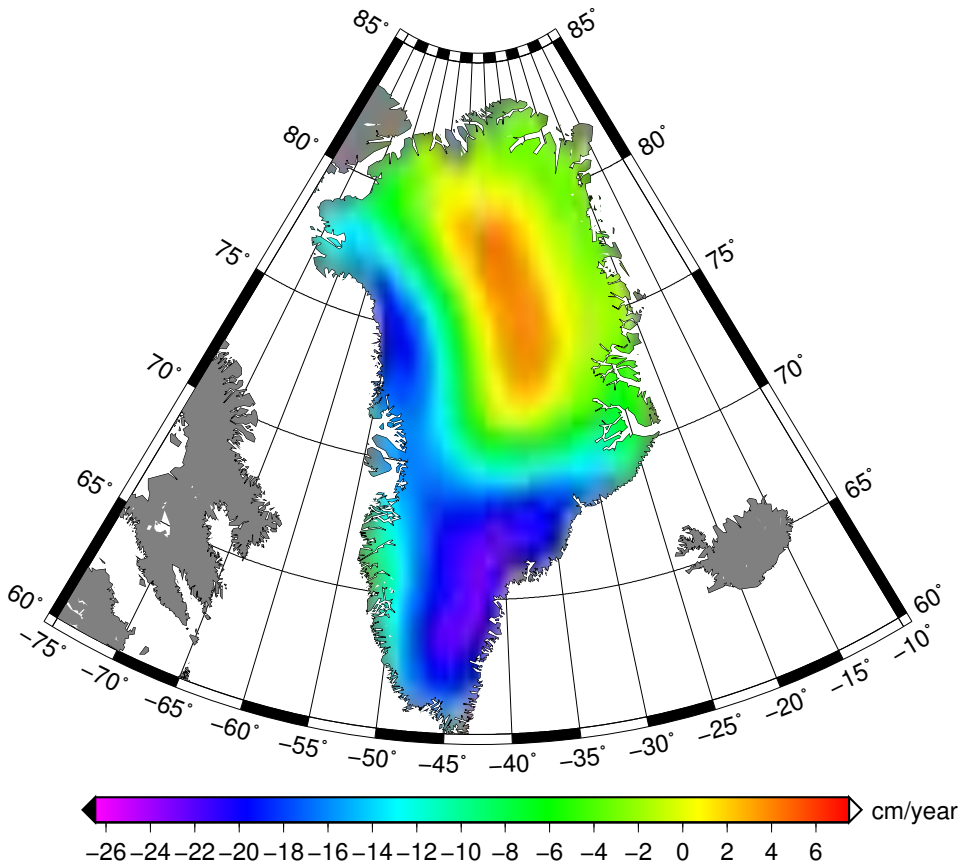
Figure 4.9: Greenland ice mass balance in the period 2003-2012 based on Level 2 GRACE data from JPL

4.4.2 Results from the GFZ models

If we compare the 2007 results of JPL with the same period computed from GFZ data, the general picture is the mainly same; see Figure 4.10. However, the GFZ data shows a more severe mass loss in the south-east and a slightly weaker ice gain in the north-east. The small area of ice gain on the west coast around $\phi = 65°$ is practically identical between JPL and GFZ. Also very similar is the area of loss on the west coast at $\phi = 75°$.
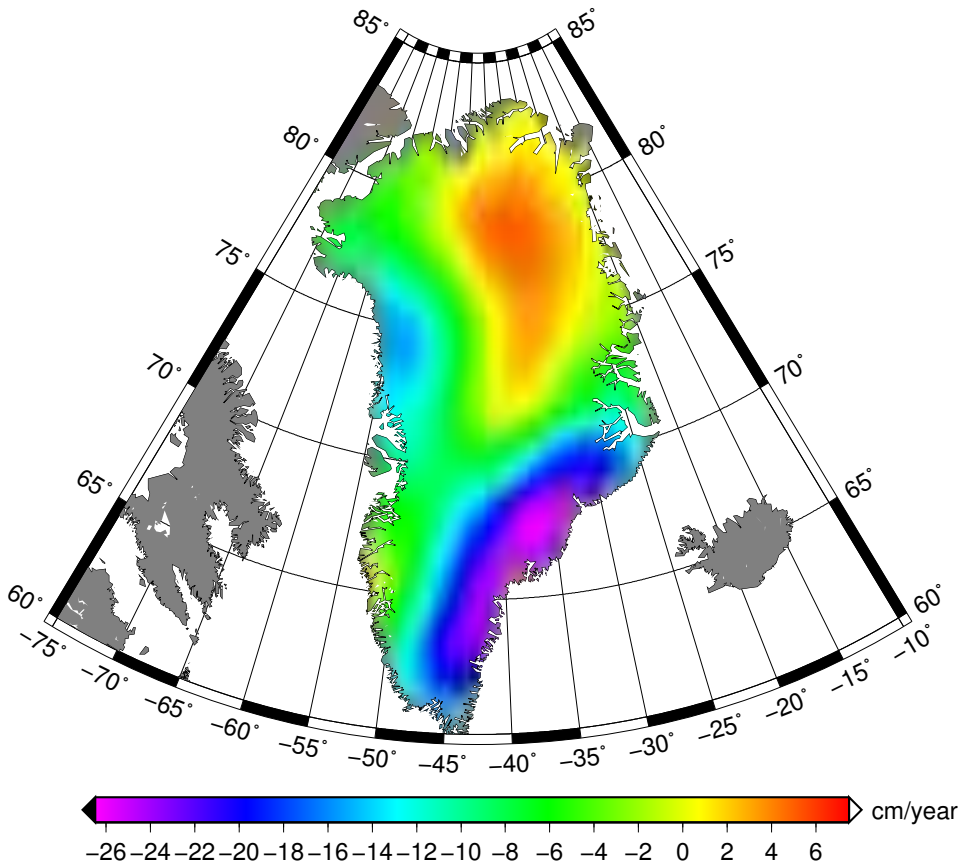
Figure 4.10: Greenland ice mass balance in the period 2003-2007 based on Level 2 GRACE data from GFZ

When comparing the GFZ 2010 data with the GFZ 2007, we can observe quite a similar trend as when we compared JPL 2007 to JPL 2010. The magnitude of the ice melt in the south-east is smaller, but the ice melt is generally spreading westwards, and significantly increasing in the area on the west coast at $\phi = 75°$. The ice gain area in the central northern part of Greenland is retracting and only a very small area is now gaining mass according to the GFZ RL05 data in the period 2003–2010. These observations can be seen in Figure 4.11.
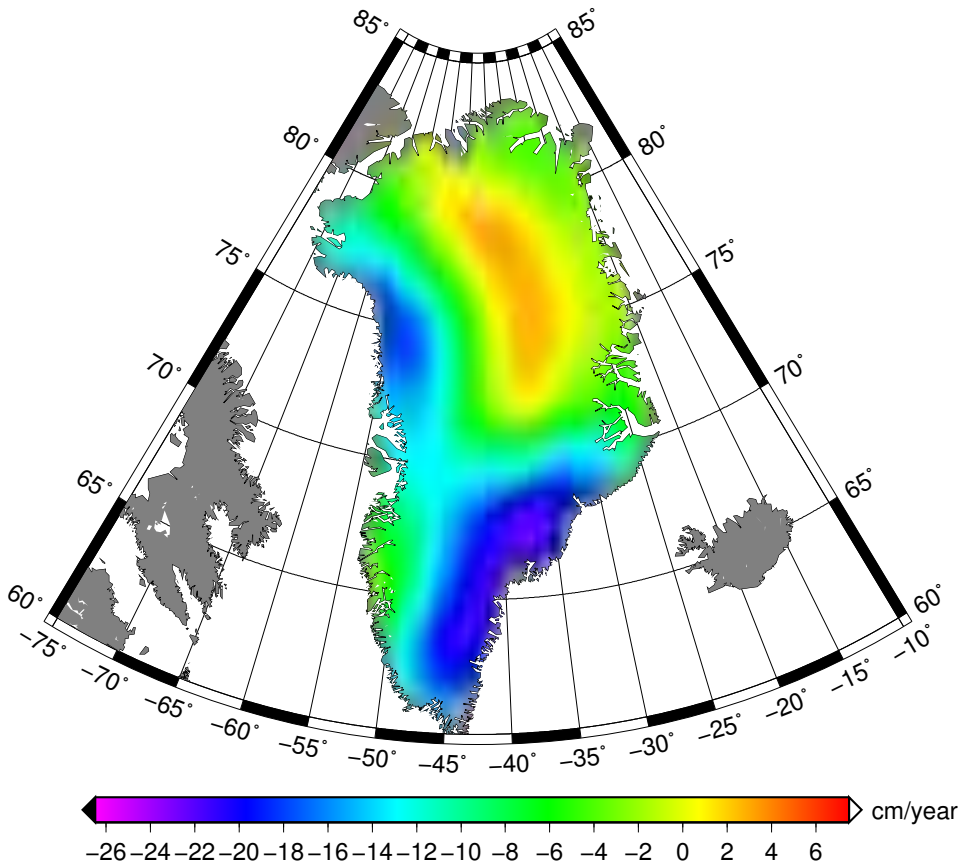
Figure 4.11: Greenland ice mass balance in the period 2003-2010 based on
Level 2 GRACE data from GFZ

The last plot in the GFZ series covers the entire period 2003–2012, and
we can recognize the trend from the JPL models: The ice loss is spreading
westwards. This can be seen in Figure 4.12. The only difference the author
can find between the transition from GFZ 2010 – 2012 compared to the
transition JPL 2010 – 2012 is that the ice gain area in the central north is
growing slightly stronger. At the same time, the ice loss in the south-east
area is getting significantly stronger in this period. If we compare the GFZ
2012 figure with the JPL 2012 figure, they look similar with slightly more
ice loss on the west coast at $\phi = 70°$ in GFZ 2012, but also slightly more ice
loss in the south-east.
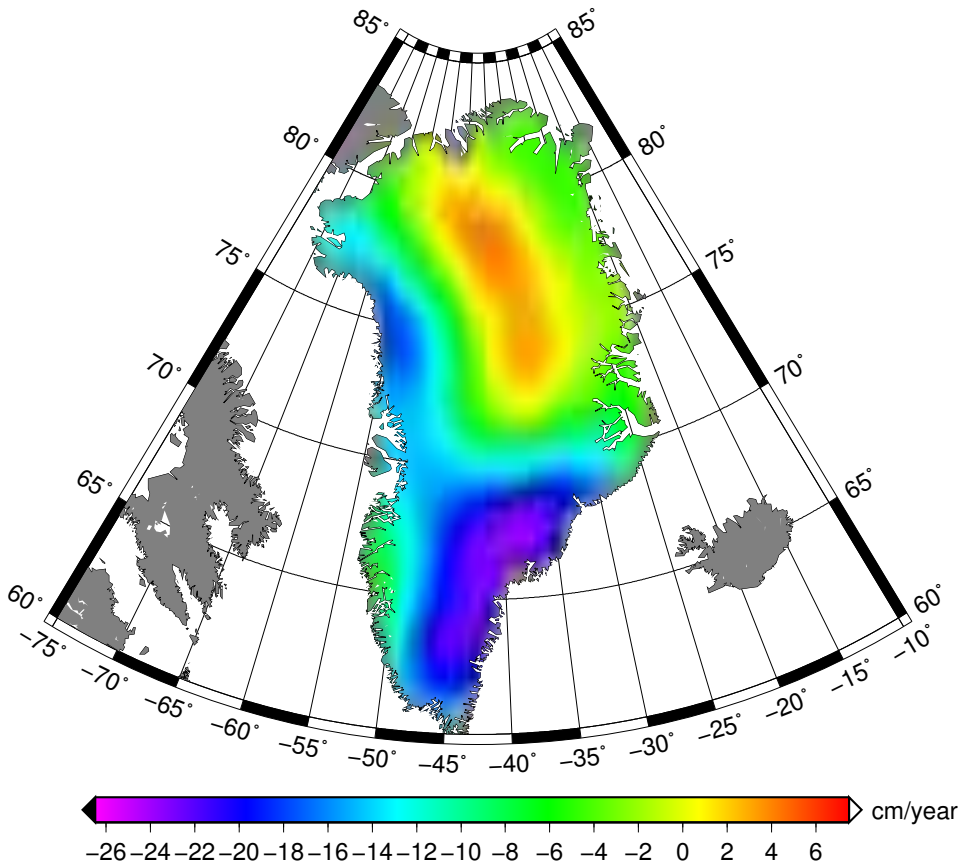
Figure 4.12: Greenland ice mass balance in the period 2003-2012 based on Level 2 GRACE data from GFZ

4.4.3 Results from the CSR models

The last provider of Level 2 GRACE data in this study is CSR. Initially, we compare the plot through 2007 with the similar data sets from JPL and GFZ, see Figure 4.13. We can see that the magnitude of the ice gain in the north is comparable to that of GFZ 2007 and smaller than that of JPL 2007. At the same time, the central northern ice gain area shares its eastern boundary with JPL2007, but the gain area does not reach just as far out to the coast in GFZ2007 compared to JPL2007. The trends along the west coast are very similar to the ones we see in both the other 2007 models. The
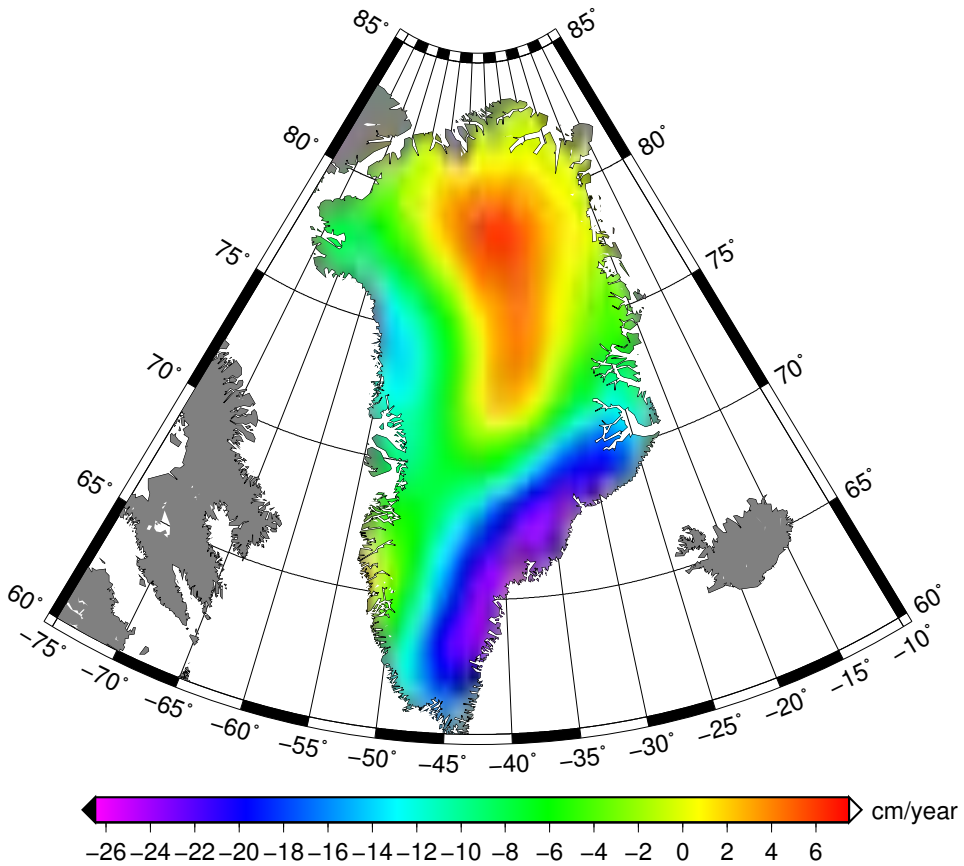
Figure 4.13: Greenland ice mass balance in the period 2003-2007 based on Level 2 GRACE data from CSR

massive ice loss area in the south-east is greater than that of JPL but weaker than that of GFZ. The boundary of this area is close to what wee see in both the other models, and the rest of the island (the green fill between the hot or cold zones) is experiencing an ice loss that is very similar to those of both GFZ and JPL.

When comparing CSR data in the period 2003–2007 with the period 2003–2010, we find a very similar pattern as in the same periods with data from GFZ and JPL: The ice gain in the central north is in decline and the most rapidly melting areas in the south-east are reducing the ice melt magnitude, but is instead spreading westwards. The new ice loss area on the west coast
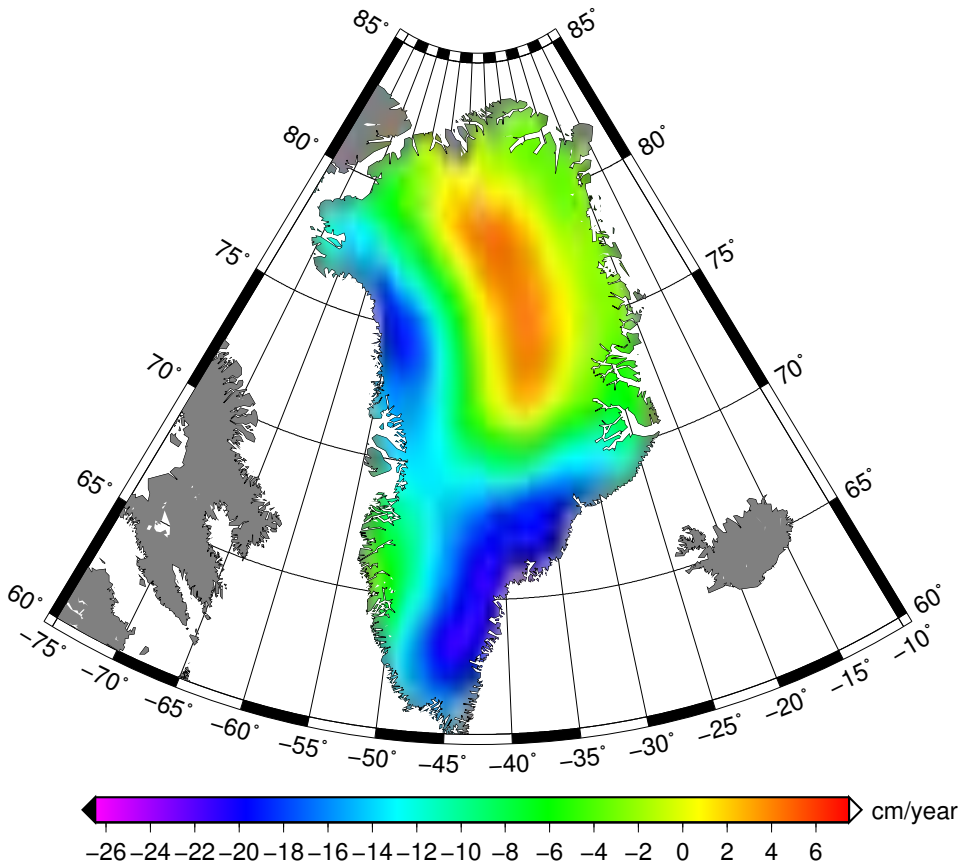
Figure 4.14: Greenland ice mass balance in the period 2003-2010 based on Level 2 GRACE data from CSR

at $\phi = 75°$ shows a great resemblance with both GFZ and JPL. This is represented in Figure 4.14.

The last figure in the sequence is Figure 4.15. It shows the CSR plot through the entire period, 2003–2012. We can recognize many of the same patterns as with JPL and GFZ, notably the increased ice loss in the south-east and the continuing spread towards the west. At the same time, the CSR model shares the result of GFZ in which the northern central area ice gain is increasing. JPL deviates in this respect, where the same area seems to recline even further when one include the 2011 and 2012 data. This detail is; however, probably unimportant compared to the more prominent

features. The difference is too small to conclude which model(s) give the best estimation on the northern central mass gain. On the other hand, there seems to be little doubt that the mass loss is real in the south and that it is moving westward.
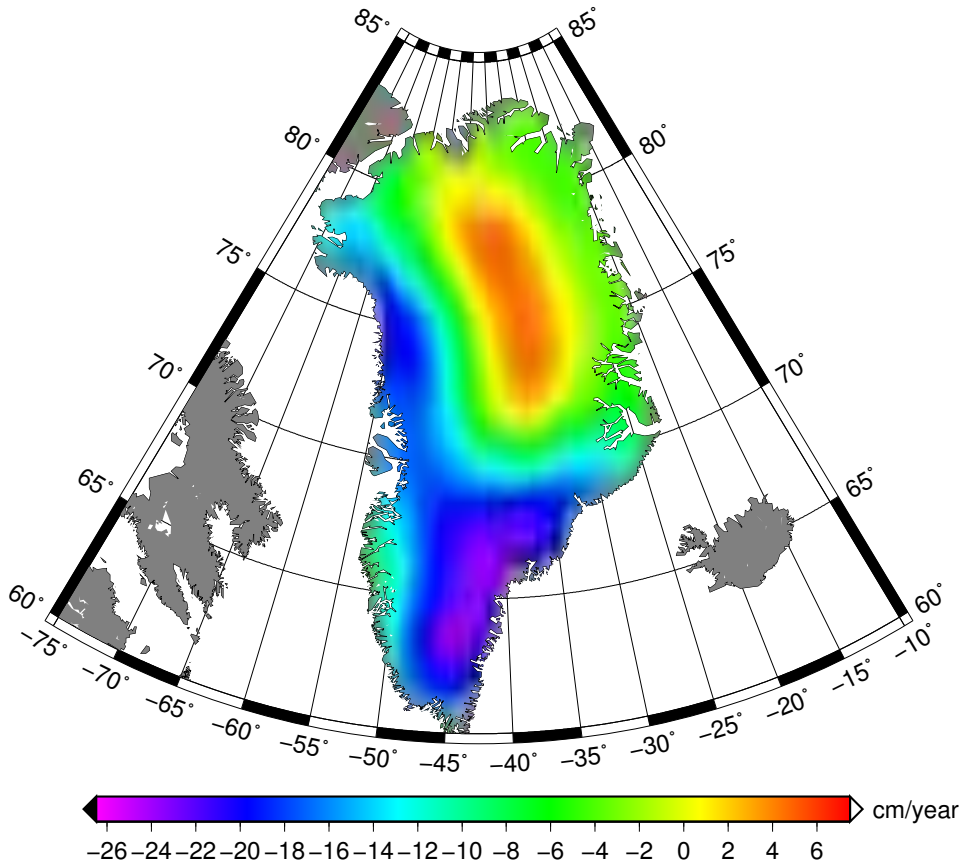
Figure 4.15: Greenland ice mass balance in the period 2003-2012 based on Level 2 GRACE data from CSR

4.5 Considerations and comparisons

In this section, we discuss further the results presented in the previous section. Let us first define some areas of special interest. Figure 4.16 identifies three interesting areas drawn over an arbitrary model from the previous section. These areas are defined as (1) the north-east gain area, (2) the western coast loss and (3) the westward expanding south-east coast. Note that the scale and unit is omitted from Figure 4.16, as its only purpose is identifying areas where we observe changes.
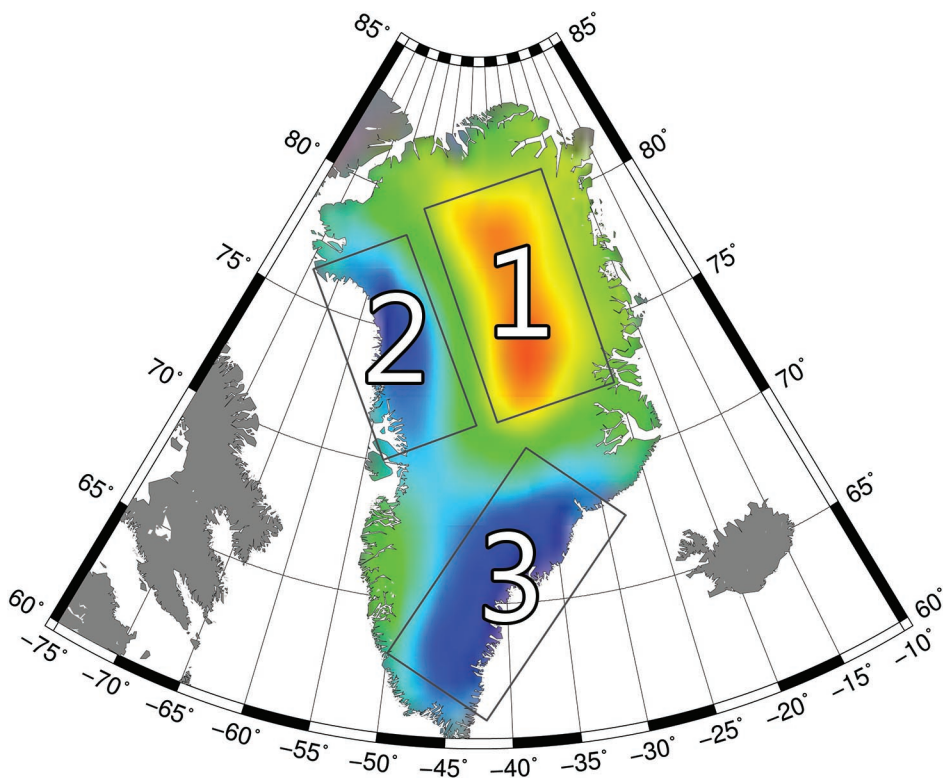
Figure 4.16: Three selected areas of special interest with regards to mass balance on Greenland

There are some conclusions that can be drawn from the time series in section 4.4. Some are more apparent and clear than others. One very uncertain tendency is that the gain area (1) might be increasing again. The JPL

model suggests that this area is slightly weakening, and the CSR model is inconclusive. GFZ shows a clearer tendency of ice mass growth. Even if this is true, it is not nearly enough to equal out the loss that we observe in the other interest areas. In the western areas around (2), there is little doubt that the mass loss is expanding in both extent and magnitude. Especially in the southbound direction, this area is expanding and is starting to merge with the south-eastern ice melt area. Moreover, the south-eastern mass loss area (3) is most likely expanding westwards. Even though the models suggested that the magnitude of the ice loss was declining in the 2010-models, it now seems to be back to the same levels as in the 2007 plots.

Let us now have a look at the secular trend for all of Greenland. Figure 4.17 shows the temporal change in the mass of Greenland measured in Gigatons. Figure 4.17 illustrates a high degree of correlation between the

Figure 4.17: GRACE estimation of time series for Greenland ice mass balance in Gigaton for the period from January 2003 to December 2012

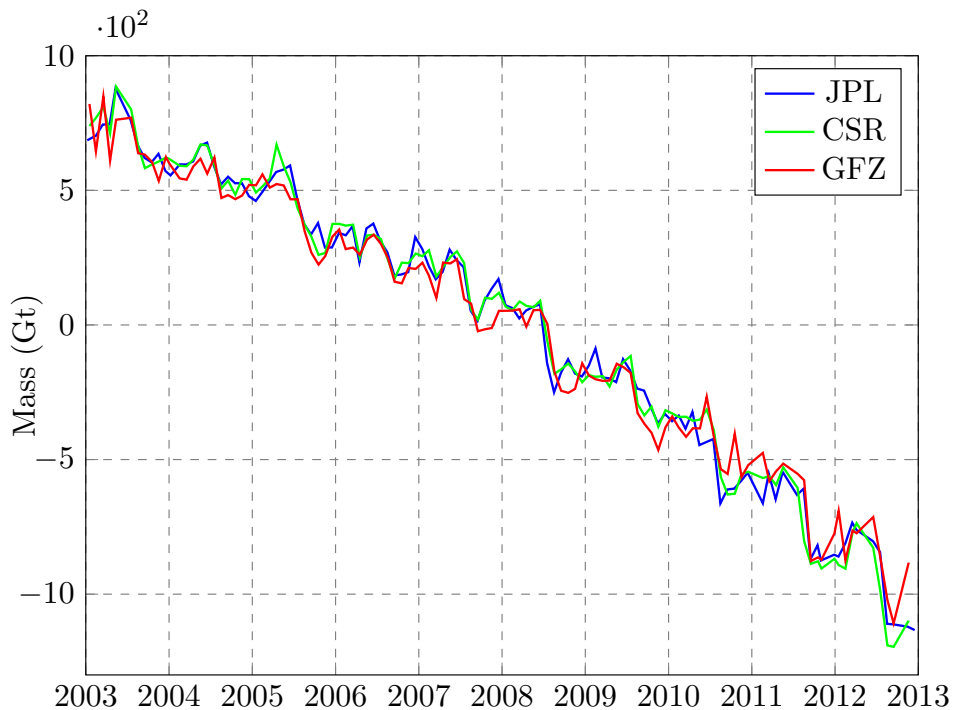three providers of Level 2 data in RL05. Especially JPL now shows a far better similarity with the other models than in previous releases. From this point, one can estimate the first order slope simply by using the least squares method for over-determined systems. The results of these computations are presented in Table 4.1. Also in this table are the results of the work of previous researchers.

Table 4.1: Ice mass change and acceleration where applicable on Greenland using GRACE data computed by different authors

Authors	Time span	Mass Change	Acceleration
Ramillien et al. [24]	2002-2005	-109±9 $^{Gt}/_{yr}$	–
Chen et al. [7]	2002-2005	-219±21 $^{Gt}/_{yr}$	–
Lutchke et. al. [20]	2003-2005	-101±16 $^{Gt}/_{yr}$	–
Velicogna and Wahr [35]	2002-2006	-227±33 $^{Gt}/_{yr}$	–
Wouters et. al. [40]	2003-2008	-179±25 $^{Gt}/_{yr}$	–
Baur et. al. [3]	2002-2008	-162±11 $^{Gt}/_{yr}$	–
Velicogna [33]	2002-2009	-230±33 $^{Gt}/_{yr}$	30±11 $^{Gt}/_{yr^2}$
Joodaki & Nahavandchi [17]	2002-2010	-163±20 $^{Gt}/_{yr}$	–
Joodaki & Nahavandchi [17]	2002-2011	-166±20 $^{Gt}/_{yr}$	32±6 $^{Gt}/_{yr^2}$
Current study JPL	2003-2012	-181±11 $^{Gt}/_{yr}$	–
Current study GFZ	2003-2012	-172±10 $^{Gt}/_{yr}$	–
Current study CSR	2003-2012	-183±11 $^{Gt}/_{yr}$	–

The methods used in this study are similar to those of Joodaki and Nahavandchi [17]. The annual mass change in this study was also computed for data in the period 2003–2012, so to compare the results with those of Joodaki and Nahavandchi [17]. The annual mass change in this experiment resulted in -164±11 $^{Gt}/_{yr}$. This is very close to their results, and can hopefully contribute to the credibility of this thesis. The actual difference, especially in the uncertainty, can probably be attributed the fact that this project uses RL05 data, while Joodaki and Nahavandchi used RL04 data. Another contribution to the difference can be that they used data spanning from January 2002, while this study uses data from January 2003. This was a deliberate choice, based on the big gaps in GRACE data during the mission's first year.

4.6 Increased compliance of JPL agaist GFZ and CSR in RL05

A very interesting observation indeed, is the increased similarity between JPL and the two other data providers. Joodaki for instance, found in his PhD thesis that the secular trend computed from JPL differs quite substantially from GFZ and CSR. This can be seen in Figure 4.2 on page 38 in his thesis [16]. This has also been found by others [3, 28]. Joodaki's results are summarized in Table 4.2. Note that the annual mass loss computed with JPL is just over 50 % compared to the GFZ and CSR.

Table 4.2: Mass balance estimated from GRACE monthly gravity field solutions provided by CSR, GFZ and JPL. Table courtesy of Joodaki [16]

Level 2 Data	Mass Balance $^{Gt}/_{yr}$
CSR	-163±20
GFZ	-161±21
JPL	-84±26

It has not been put any effort into determining why the JPL data differs from GFZ and CSR in RL04 and earlier, but according to this study, the deviation seems to be completely eliminated in RL05. Of course, it is too early to draw any conclusions based only on this project, but it now seems that JPL data can be used equally with GFZ and CSR. NASA still say that JPL is only supposed to be used for verification purposes, but at least it will be interesting to see if other studies can find the same trend with RL05 data. At the same time, it is interesting to note that Joodaki found the CSR model and the GFZ model to be very close to each other with 161±21 and -163±20 Gigatons per year respectively. In this study, GFZ was the one model to stand out at -172±10 versus -181±11 and -183±11 Gigatons per year for JPL and CSR. From Figure 4.17, this might seem to arise from the very last part of the data set, where the GFZ model estimates a greater mass gain than the two other models. It is not known which is more correct, but hopefully later studies will reveal the truth.

4.7 Reconsidering spatial resolution

Earlier in this thesis, the maximum frequency l_{max} has been discussed. The available data has been either up to degree and order 60 or 90, and 60 has been chosen. Eq. 2.20 suggests a resolution of 360, as seen on page 30. This was never an option, but one thing was never considered: Could the spatial resolution be reduced to accommodate the eq. 2.20? By solving the formula for $l_{max} = 60$, we get a suggested resolution of

$$ O^\circ = \frac{180^\circ}{60} = 3^\circ. $$

This would definitely save computing time, as there would have been $\left({}^{0.5^\circ}/{}_{3^\circ} \right)^2 = {}^1/{}_{36}$th as many points. This in turn yields a total of $2541 \times 36^{-1} \approx$ 70 points inside Greenland. For the northern cap region, the relative reduction would not be quite as big, since this already was computed on a 1° grid, but it would still reduce the number of points from 10800 to 1800 – a great contribution to reducing computing time for the leakage effect.

At the same time, a spatial resolution purely based on the above "rule of thumb" formula would probably be too small. Even if this is the suggested resolution from the pure GRACE data truncated at degree and order 60, it does not take into account the smoothing filtering that are applied afterwards. When the signal is smoothed, we again gain relevant information in the originally coarse resolution. It has not been conducted any further research into investigating the effect of reducing the spatial resolution, but for further research, it can be advisable to test this, for instance by comparing the results of a computation done at spatial resolution of 0.5° with a computation done at 1° resolution.

Table 4.3: Minimum and maximum values in annual ice mass loss in cm from the models by JPL, GFZ and CSR

Model	Min	Max
JPL 2003–2007	-23.80 cm/yr	6.04 cm/yr
JPL 2003–2010	-20.53 cm/yr	4.79 cm/yr
JPL 2003–2012	-23.03 cm/yr	5.61 cm/yr
GFZ 2003–2007	**-26.30** cm/yr	5.30 cm/yr
GFZ 2003–2010	-22.32 cm/yr	3.18 cm/yr
GFZ 2003–2012	-23.89 cm/yr	4.47 cm/yr
CSR 2003–2007	-24.51 cm/yr	**6.60** cm/yr
CSR 2003–2010	-21.10 cm/yr	5.25 cm/yr
CSR 2003–2012	-23.60 cm/yr	4.54 cm/yr

Chapter 5

Concluding remarks

In this thesis, we have seen that the trend of the previously observed Greenland ice melt is continuing. The ice cap of this vast island is losing mass, maybe faster than ever before in modern history. This is based on computations of 12 whole years of GRACE satellite data. Especially three areas seem to have a high activity. The north-eastern part of the island has previously seen a gain in the ice mass, but this trend has currently stagnated or maybe even declined. In the south-east, we saw a great mass loss in the data set when measuring with data in the time range 2003–2007. When we included data through 2010, this decline had reduced in magnitude, but spread in extent. With the latest 2012 data, the magnitude of the decline in ice loss is now greater again, and the extent is continuing to the third active region; the west coast. Previously, we saw a slight mass gain on the southern west coast, but this area has now come under the effect of the eastern mass loss spreading westwards. In the north-west, the ice is also melting faster than we have seen before. Table 4.1 shows that estimation of mass change was very inconclusive in the first years, but may now, to an increasing degree, be converging. More research is of course needed to become more certain of this.

The findings in this thesis are based on state of the art satellite technology and the latest techniques for preprocessing the satellite data. Other strengths

of the study are close correlation of results when computing similar time series as have been previously been done by other researchers, and the separation of leakage in and leakage out signal. This has been pointed out by Baur et al. [3] as an advantage, as opposed to estimating the total leakage in the target area in one process. It is also pleasant to see the increased coherence between GFZ, CSR and JPL in RL05 compared to results published before with RL04 data. This was expected, based on the findings of for instance Bettadpur [5].

On the other hand, as the results from different researchers are still too far apart to enable us to determine with certainty the magnitude of the ice melt, we cannot fully evaluate the performance of this thesis with respect to the correctness of the results. These differences can originate and propagate from several reasons. Different approaches to handling the GRACE Level 2 data, different ways (or omitting) of post-glacial rebound and gravity leakage corrections, truncation of signal at a different frequency, spatial resolution, and earlier releases of GRACE Level 2 data can all contribute to these variations.

There are several things that could have been done to improve this study as well. An investigation of the effect of reducing the spatial resolution could save computing time in later research if the results turned out to be equally good. It was unfortunately no time to test the effect of resolution reduction during this project. It could also be interesting to see if a substitution of the C_{20} coefficients would have any noticeable effect on the final results. Replacing the coefficients is easy – the code was written but later commented out, but the computation time with the current spatial resolution was too time consuming. A thorough investigation into whether to include correction for post-glacial rebound was not conducted to estimate the differences of various models. There are also several different methods of estimating the errors, both systematic and random. To achieve a better estimate, it can be useful to look into different methods. This has not been done in this study.

The final thing to note is the assumption of the area on Greenland. This has been estimated to $2.166 \cdot 10^6$ km^2 [1]. In this study, the area was set to

2.055·10^6 km^2. The difference in these numbers arise from the computing of the area in this thesis. This was not done based on the (relatively accurate) shape file included in Matlab, but instead on a polygon surrounding the 2541 points selected on Greenland. Since the points in this polygon are used in the computations of $\Delta\sigma$, this is also the area one must use to estimate the annual mass loss of Greenland. Even if the difference in the two ways of measuring the area has a difference of $^{2.166}/_{2.055}\approx 5\%$, the error in the total estimation is far less than this.

As far as the author's knowledge reaches, no other studies have so far been published that estimates the mass balance on Greenland using GRACE RL05 data that has been decorrelated with a non-isotropic filter. This study is by no means the end of the research. New information is being released rapidly, and new techniques for better assessments are developed in a fast pace. Hopefully, upcoming research will show a tendency of converging results.

Bibliography

[1] Central Intelligence Agency. The world factbook. `http://cia.gov/library/publications/the-world-factbook/`, 2013.

[2] W Yu Anthony, Michael A Krainak, Mark A Stephen, James B Abshire, David J Harding, Haris Riris, Steven X Li, Jeffrey R Chen, Graham R Allan, Kenji Numata, et al. Spaceflight laser development for future remote sensing applications. In *Remote Sensing*, pages 818204–818204. International Society for Optics and Photonics, 2011.

[3] O Baur, Michael Kuhn, and WE Featherstone. Grace-derived ice-mass variations over greenland by accounting for leakage effects. *Journal of Geophysical Research: Solid Earth (1978–2012)*, 114(B6), 2009.

[4] S Bettadpur. Level-2 gravity field product user handbook. *GRACE 327*, 734, 2007.

[5] S Bettadpur. Insights into the earth system mass variability from csr-rl05 grace gravity fields. In *EGU General Assembly Conference Abstracts*, volume 14, page 6409, 2012.

[6] DP Chambers and JA Bonin. Evaluation of release-05 grace time-variable gravity coefficients over the ocean. *Ocean Science Discussions*, 9(3):2187–2214, 2012.

[7] JL Chen, CR Wilson, and BD Tapley. Satellite gravity measurements confirm accelerated melting of greenland ice sheet. *Science*, 313(5795):1958–1960, 2006.

63

[8] Minkang Cheng and Byron D Tapley. Variations in the earth's oblateness during the past 28 years. *Journal of geophysical Research*, 109(B9):B09402, 2004.

[9] Christoph Dahle, Frank Flechtner, Christian Gruber, Daniel König, Rolf König, Grzegorz Michalak, and Karl-Hans Neumayer. Gfz rl05: An improved time-series of monthly grace gravity field solutions. In *Observation of the System Earth from Space-CHAMP, GRACE, GOCE and future missions*, pages 29–39. Springer, 2014.

[10] Bruce Douglas, Mark T Kearney, and Stephen P Leatherman. *Sea level rise: History and consequences*, volume 75. Access Online via Elsevier, 2000.

[11] A Geruo, John Wahr, and Shijie Zhong. Computations of the viscoelastic response of a 3-d compressible earth to surface loading: an application to glacial isostatic adjustment in antarctica and canada. *Geophysical Journal International*, 192(2):557–572, 2013.

[12] Vivien Gornitz. Sea-level rise: A review of recent past and near-future trends. *Earth Surface Processes and Landforms*, 20(1):7–20, 1995.

[13] JY Guo, ZW Huang, CK Shum, and W van der Wal. Comparisons among contemporary glacial isostatic adjustment models. *Journal of Geodynamics*, 61:129–137, 2012.

[14] Lars Hernquist and Martin D Weinberg. Simulations of satellite orbital decay. *Monthly Notices of the Royal Astronomical Society*, 238:407–416, 1989.

[15] E Holzschuh, W Kündig, et al. Determination of the gravitational constant with a beam balance. *Physical review letters*, 89(16):161102, 2002.

[16] Gholamreza Joodaki. *Earth Mass Change Tracking Using GRACE Satellite Gravity Data*. PhD thesis, Norwegian University of Science and Technology, 2013.

[17] Gholamreza Joodaki and Hossein Nahavandchi. Mass loss of the greenland ice sheet from grace time-variable gravity measurements. *Studia Geophysica et Geodaetica*, 56(1):197–214, 2012.

[18] Jürgen Kusche, Roland Schmidt, S Petrovic, and Roelof Rietbroek. Decorrelated grace time-variable gravity solutions by gfz, and their validation using a hydrological model. *Journal of geodesy*, 83(10):903–913, 2009.

[19] Kristine M Larson, Neil Ashby, Christine Hackman, and Willy Bertiger. An assessment of relativistic effects for low earth orbiters: the grace satellites. *Metrologia*, 44(6):484, 2007.

[20] Scott B Luthcke, HJ Zwally, W Abdalati, DD Rowlands, RD Ray, RS Nerem, FG Lemoine, JJ McCarthy, and DS Chinn. Recent greenland ice mass loss by drainage system from satellite gravity observations. *Science*, 314(5803):1286–1289, 2006.

[21] Isabelle Panet, Valentin Mikhailov, Michel Diament, Fred Pollitz, Geoffrey King, Olivier De Viron, Matthias Holschneider, Richard Biancale, and Jean-Michel Lemoine. Coseismic and post-seismic signatures of the sumatra 2004 december and 2005 march earthquakes in grace satellite gravity. *Geophysical Journal International*, 171(1):177–190, 2007.

[22] Nikolaos K Pavlis, John K Factor, and Simon A Holmes. Terrain-related gravimetric quantities computed for the next egm. In *Proceedings of the 1st International Symposium of the International Gravity Field Service (IGFS), Istanbul*, pages 318–323, 2007.

[23] WR Peltier. Global glacial isostasy and the surface of the ice-age earth: The ice-5g (vm2) model and grace. *Annu. Rev. Earth Planet. Sci.*, 32:111–149, 2004.

[24] G Ramillien, A Lombard, A Cazenave, ER Ivins, M Llubes, F Remy, and R Biancale. Interannual variations of the mass balance of the antarctica and greenland ice sheets from grace. *Global and Planetary Change*, 53(3):198–208, 2006.

[25] M Rodell, MM Watkins, and JS Famiglietti. Remote sensing of terrestrial water storage with grace and future satellite gravimetry missions. In *AGU Fall Meeting Abstracts*, volume 1, page 05, 2011.

[26] R Schmidt, F Flechtner, U Meyer, K-H Neumayer, Ch Dahle, R König, and J Kusche. Hydrological signals observed by the grace satellites. *Surveys in Geophysics*, 29(4-5):319–334, 2008.

[27] S Solomon, D Qin, M Manning, Z Chen, M Marquis, K.B. Averyt, M. Tignor, and H L Miller. Climate change 2007: The physical science basis. contribution of working group i to the fourth assessment report of the intergovernmental panel on climate change. Technical report, United Nations, 2007.

[28] L Sandberg Sørensen and René Forsberg. Greenland ice sheet mass loss from grace monthly models. In *Gravity, Geoid and Earth Observation*, pages 527–532. Springer, 2010.

[29] Sean Swenson and John Wahr. Methods for inferring regional surface-mass anomalies from gravity recovery and climate experiment (grace) measurements of time-variable gravity. *Journal of Geophysical Research: Solid Earth (1978–2012)*, 107(B9):ETG–3, 2002.

[30] Sean Swenson and John Wahr. Post-processing removal of correlated errors in grace data. *Geophysical Research Letters*, 33(8):L08402, 2006.

[31] Sean Swenson, John Wahr, and PCD Milly. Estimated accuracies of regional water storage variations inferred from the gravity recovery and climate experiment (grace). *Water Resources Research*, 39(8), 2003.

[32] Byron D Tapley, Srinivas Bettadpur, John C Ries, Paul F Thompson, and Michael M Watkins. Grace measurements of mass variability in the earth system. *Science*, 305(5683):503–505, 2004.

[33] Isabella Velicogna. Increasing rates of ice mass loss from the greenland and antarctic ice sheets revealed by grace. *Geophysical Research Letters*, 36(19), 2009.

[34] Isabella Velicogna and John Wahr. Greenland mass balance from grace. *Geophysical Research Letters*, 32(18), 2005.

[35] Isabella Velicogna and John Wahr. Acceleration of greenland ice mass loss in spring 2004. *Nature*, 443(7109):329–331, 2006.

[36] C Wagner, D McAdoo, J Klokočník, and J Kosteleckỳ. Degradation of geopotential recovery from short repeat-cycle orbits: application to grace monthly fields. *Journal of Geodesy*, 80(2):94–103, 2006.

[37] John Wahr, Mery Molenaar, and Frank Bryan. Time variability of the earth's gravity field: Hydrological and oceanic effects and their possible detection using grace. *Journal of Geophysical Research*, 103(B12):30205–30, 1998.

[38] John Wahr and Isabella Velicogna. What might grace contribute to studies of post glacial rebound? In *Earth Gravity Field from Space—From Sensors to Earth Sciences*, pages 319–330. Springer, 2003.

[39] David N Wiese, WM Folkner, and RS Nerem. Alternative mission architectures for a gravity recovery satellite mission. *Journal of Geodesy*, 83(6):569–581, 2009.

[40] B Wouters, D Chambers, and EJO Schrama. Grace observes small-scale mass loss in greenland. *Geophysical Research Letters*, 35(20), 2008.